NASA Technical Paper 1606

Orbit Dynamics and Geographical Coverage Capabilities of Satellite-Based Solar Occultation Experiments for Global Monitoring of Stratospheric Constituents

David R. Brooks

MARCH 1980

NASA

NASA Technical Paper 1606

Orbit Dynamics and Geographical Coverage Capabilities of Satellite-Based Solar Occultation Experiments for Global Monitoring of Stratospheric Constituents

David R. Brooks
Langley Research Center
Hampton, Virginia

National Aeronautics
and Space Administration

**Scientific and Technical
Information Office**

1980

A

SUMMARY

An analysis is presented for Earth-orbiting spacecraft missions designed to measure stratospheric constituents using solar occultation. This technique uses the Sun as an energy source and depends on the attenuation of solar radiation as the Sun's image rises or sets through the atmosphere as viewed from a spacecraft. The orbital mechanics of solar occultation are examined, and some results are summarized for a simulated 1-year mission using an orbit with an inclination of 70° and an altitude of 600 km. Of particular concern is the spatial and temporal atmospheric sampling relative to the Earth's surface. The nominal orbit has been chosen so that some spatial coverage can be obtained at all latitudes. There are 1 to 15 opportunities per year, depending on latitude, to make a series of consecutive measurements in the vicinity of any particular latitude. Sampling capabilities of solar occultation missions are then examined parametrically for a range of orbit conditions.

A simulated 1-year data base is presented for the nominal mission. The data consists of 9480 "measurements" of a single quantity associated with each measurement opportunity. These data are produced by a model whose underlying functional variability is not revealed. The measurements are grouped into latitude bands, and the observed variability within latitude bands is assumed to be both systematic and random. The statistical properties of the data set are examined to determine the extent to which global behavior can be extracted from solar occultation mission data. A standard curve-fitting technique is applied to these data, by which parameters are determined for a simple periodic mathematical model with variable mean, amplitude, and phase.

INTRODUCTION

Global monitoring of the stratosphere is important in attempting to understand and protect the Earth's environment. Stratospheric components of particular interest are aerosols, ozone, and many trace gases which participate in the complex photochemical processes of ozone production and depletion. These components, through their ability to scatter and absorb solar radiation, play a critical role in the Earth's radiation balance and hence in maintaining climate and weather within acceptable limits.

The use of Earth-orbiting spacecraft to provide reliable long-term global monitoring is part of a total commitment to providing the necessary data base for present and future environmental studies. One technique for measuring stratospheric constituents using a spaceborne sensing system is to measure the attenuation of solar radiation as the Sun's image rises or sets through the atmosphere. There are two monitoring opportunities per orbit, one sunrise and one sunset, except for those times when the spacecraft is in continuous line-of-sight contact with the Sun. These so-called solar occultation measurements are potentially applicable to a variety of stratospheric monitoring activities. In

one recently proposed flight experiment, the objective is to learn more about the distribution of stratospheric aerosols (ref. 1); in another proposal, the objective is to study halogens (such as HCl) in the stratosphere (ref. 2). In the former case, the proposed flight experiment attempts to expand a body of knowledge that is already quite large, to the extent that many facets of aerosol production, distribution, transport, and depletion are understood reasonably well. In the latter case, the importance of halogens in stratospheric ozone chemistry has only recently been recognized on theoretical grounds, and is unverified by direct measurements. Hence, the proposed flight experiment is only a first step toward understanding concentration levels and the coarsest features of the underlying distributions. A shared characteristic of these missions, typical of cases where solar occultation measurements are expected to be useful, is the need for global long-term coverage. This paper demonstrates how this basic requirement can be met and provides a preliminary outline of one way in which the resulting data might be used to determine the behavior of stratospheric constituents over spatial and temporal scales of interest.

The concept of "global" coverage is a flexible one which may be interpreted in different ways for meeting different objectives. For the present purposes, global coverage is interpreted to mean that all latitudes are covered by a single satellite on one or more occasions during a year. This requirement leads to orbits of high, but not necessarily polar, inclination, as shown when the orbit geometry is examined in detail. It is unfortunate that the global coverage requirement cannot be met with Sun-synchronous orbits so that solar occultation measurements would be compatible with many other types of Earth-monitoring activities, but this specialized geometry gives only restricted latitudinal coverage over a range which depends on the initial timing of the orbit with respect to the Sun. Such a case has been examined in a previous study (ref. 1), where the objective was to show how a two-satellite mission could effectively combine the coverage of a Sun-synchronous orbit with that achieved at a lower inclination.

An inherent limitation of the solar occultation technique is that the local time of day (the "clock" time) at the locations of the measurements is necessarily restricted to dawn or dusk. Thus, the technique is not capable of monitoring diurnal variations. These must either be assumed to be insignificant or be accounted for with mathematical modeling and/or data from some other source.

The overall possibilities for and limitations on spatial and temporal coverage with the solar occultation technique must be assessed on the basis of the total amount of data obtained in a specific period of time. To achieve some understanding of how such data would be accumulated, a twofold approach has been used. First, a nominal 1-year mission has been defined and its particular output examined in detail. This mission has been selected to achieve some global coverage in the sense described previously. Then, from the insight provided by a specific case, some important aspects of the nominal mission are generalized and expanded parametrically to cover a wider range of orbit options.

After the orbital analyses are complete, the nominal mission is recalled to generate a set of simulated measurements for statistical examination. For the purposes of this paper, it has been assumed that adequacy of spacecraft coverage can be investigated in terms of the extent to which spatially and temporally varying distributions can be extracted from a simulated set of single-parameter values. These data are produced by a single-valued function of longitude, latitude, and time which associates one scalar quantity (the "measurement") with each occultation opportunity. The actual process of recording a complete sunrise or sunset is much more complicated; it consists of a series of individual measurements obtained as the Sun rises or sets, each of which must then be interpreted in terms of variations in the measured quantity. One such interpretation, but certainly not the only one, would be to assume that the measurements constitute a vertical profile through the atmosphere. This involves data reduction algorithms which are of no concern for the present analysis. Further treatment of the data, such as integration over altitude, could yield a single parameter associated with each sunrise or sunset. Integrating a vertical profile could result in a total vertical burden, although other single-parameter results might also be of interest. However the data analysis is accomplished, another basic assumption of this paper is that the details are of no concern for assessing the adequacy of global coverage of the occultation events.

A third assumption about the simulated data is that for the proposed investigation of coverage capabilities with a particular spacecraft-based measurement technique, the specific origin and form of the single-parameter model is not important. It can produce any set of values whose spatial and temporal variability includes and exceeds that which can be extracted from the resulting data base. In this paper the model is thought of as a "black box" incorporated into a computer program for orbit propagation. At each sunrise or sunset, the appropriate space and time coordinates are input to the model, which returns a single value. It might be desirable to have this scheme produce output which an experimenter can relate to his expectations and past experience, but this is not necessary. The details of the model used in this paper are not discussed at all, but are revealed only through the measurements simulated in the nominal mission. This approach is an accurate representation of the real environment wherein underlying distributions of observed quantities are revealed piecemeal through the measurements which are available. Any other approach would place unwarranted emphasis on the suitability of the model for predicting the actual behavior of a physical quantity - a goal which is totally beyond the scope of this study.

In the statistical analysis of the data set, two different procedures are followed. First, some descriptive statistical parameters are calculated, mean values, for example, and confidence limits are discussed for this type of information obtained with no knowledge of or assumptions about the functional form of the variability in the data. Second, some assumptions are made about the data in the form of a simple periodic model, and three parameters - mean, amplitude, and phase - are fitted to the data. Confidence in this process is then related to the amount of the total observed variability which can be represented by the model, without regard to its physical basis.

SYMBOLS

a	semimajor axis, km
A	amplitude, one of three parameters in a model for $\bar{q}$, units of q
$\underline{B}$	coefficient matrix in the model for $\bar{q}$
B,b,c,d	angles, defined in figure 10, needed to calculate λ_T given i, h, and δ_Θ, deg
$\underline{C}$	matrix of parameters C_1, C_2, and C_3 to be estimated by the least squares technique in the model for $\bar{q}$
D	central angle between a spacecraft and the Earth's horizon, deg
f	true anomaly, deg
h	altitude, km
$\hat{H}$	unit heading vector (see fig. 2)
i	inclination, deg; also, a summation index
L	longitude, deg
$\underline{M}$	matrix of observations of $\bar{q}$
n	number of values in a sample for statistical analysis
$\hat{N}$	unit vector perpendicular to a spacecraft orbit (see fig. 2)
P_T	point on the surface of a spherical Earth at which solar occultation measurement is made
q	single parameter assumed to have been extracted from a series of measurements taken at sunrise or sunset, expressed in arbitrary units
$\bar{Q}$	sample mean calculated from a set of $\bar{q}$'s, units of q
Q	mean, one of three parameters in a model for $\bar{q}$, units of q
$\vec{r}$	spacecraft position vector from the center of the Earth, km
$\vec{r}_T$	position vector of tangent point from center of Earth
r_Θ	radius of Earth, 6378.145 km
R	ratio which determines how well variability in data has been represented

RA	right ascension, deg
s^2	sample variance, units of q^2
$\vec{S}$	vector in direction of $\hat{x}_\Theta$ defined in equation (1)
SC	spacecraft
t	time, days, or dimensionless ratio normalized to 1 year
v	velocity, km/sec
$\hat{x}_\Theta$	unit vector to the Sun
Y	an arbitrary observed quantity
α,β	pointing angles to the Sun referenced to a spacecraft coordinate system $(\hat{H},\hat{N},\hat{r})$, deg
γ	phase factor, one of three parameters in a model for $\bar{q}$, deg
δ	declination, deg
ϵ	residual error in a model for $\bar{q}$, units of q
η	angle defined as $90^\circ + \delta_\Theta$ (see eq. (5)), deg
λ	latitude, deg
μ	actual mean (unknown) of a population whose mean is to be estimated from observations made on the population, units of q
Υ	direction of the vernal equinox vector, for locating the x-axis of an Earth-equatorial (right-ascension–declination) coordinate system
ω	argument of perigee, deg
Ω	right ascension of ascending node, deg

Subscripts (not defined in main symbol list):

rel	relative to the horizon at the time of a sunrise or sunset
R	residuals, as when calculating the sum of squares of the residuals
T	tangent point at the surface of a fictitious spherical Earth or on a concentric spherical shell around the Earth
TG	tangent point referenced to the surface of an ellipsoidal Earth
Θ	referring to the Sun

Notation:

$\rightarrow$ dimensioned vector

$\hat{}$ unit vector; or to denote estimates of the value of scalar quantities

$\bar{}$ averaged quantity obtained from a set of observations

THE ORBIT DYNAMICS OF SOLAR OCCULTATION MISSIONS

The well-known precession of a spacecraft orbit plane, as predicted by first-order perturbation theory (ref. 3), is of dominant interest for the analysis of solar occultation missions. Both the argument of perigee ω and right ascension of the ascending node Ω are functions of time. This changing Sun–orbit-plane geometry determines the limits on and rates of spatial coverage. The geometry for characterizing a sunrise or sunset viewed from Earth orbit is defined in figure 1. All the vectors are expressed in a right-ascension–declination (RA-δ) system, which is an Earth-equatorial system with the x-axis in the direction of the vernal equinox vector (Υ). The unit vector $\hat{x}_\odot$ points from the spacecraft to the center of the Sun. The orbit plane is located in space by its inclination to the equator i and by the angular elements ω and Ω. The spacecraft is located within an orbit by its true anomaly f, the angular distance between perigee and spacecraft. A sunrise or sunset occurs, by definition, at that instant at which the projection of $\hat{x}_\odot$ is tangent to the surface of a spherical Earth at P_T; the position vector to P_T is $\vec{r}_T$, with longitude and latitude coordinates L_T and λ_T. (This differs from the usual astronomical definition of sunrise or sunset as viewed from the ground, but it is an appropriate choice for this study. It can be modified if necessary to account for the oblateness of the Earth and other contributions to a variation in the actual location of the horizon as viewed from the spacecraft.)

The first step in locating the tangent points is outlined in appendix A. (This appendix has previously been published as appendix C of ref. 3; it is included here for completeness.) A derivation is given for finding the orbit true anomalies at which occultations occur. Given such a point on the orbit, its radius vector $\vec{r}$ (in the RA-δ system) can be found (see, for example, ref. 3). Then, from simple geometrical considerations, $\vec{r}_T$ is the vector sum of $\vec{r}$ and a vector $\vec{S}$, which is in the direction of $\hat{x}_\odot$ and whose magnitude is

$$|\vec{S}| = |\vec{r}| \sin\left[\cos^{-1}\left(\frac{r_\oplus}{|\vec{r}|}\right)\right] \tag{1}$$

The derivation in appendix A assumes fixed orbit elements. Since both ω and Ω are changing, some iteration is required. Fortunately, the changes in ω and Ω are only fractions of a degree per orbit. So, the procedure which has been followed is to calculate the true anomalies at which occultations occur for an orbit whose angular elements ω and Ω are fixed at the values

corresponding to the time of perigee. Then, the times from perigee to the points of occultation are used to update ω and Ω and the calculations are repeated. This one-step iteration gives occultation points to a sufficiently high degree of accuracy for the intended purpose.

Note that the maximum latitude of the tangent point can exceed the maximum subsatellite latitude and that the location of the tangent point depends simultaneously on the orbit inclination and altitude and on solar position. It is useful to think of the tangent latitude as depending predominantly on the orbit parameters and the subsolar declination and the tangent longitude as depending largely on the Earth's rotation. Consider the angular rates involved: relative to an inertial coordinate system, the Sun appears to precess at about 1 deg/day in the positive direction; an orbit of less than 90° inclination precesses in the negative direction at a typical rate of a few degrees per day, while the Earth rotates in the positive direction at 361 deg/day. Thus, it is expected that the tangent latitude would undergo a relatively slow variation as the Sun's declination changes and the orbital plane precesses, while the Earth's rotation would produce a much more rapid variation in the tangent longitude.

Turning now to the definition of the vector $\hat{x}_{\odot}$ relative to a spacecraft, figure 2 establishes a coordinate system at the spacecraft for defining pointing angles to the Sun; α is a "pitch" angle (down to the horizon for a sunrise or sunset) and β is a "yaw" angle which locates the Sun relative to the plane of the spacecraft motion. For a circular orbit and a spherical Earth, α has a constant negative value at the horizon for each orbital altitude.

Analysis of a Solar Occultation Mission

With the discussion and definitions of the previous section, a hypothetical solar occultation mission can be formulated and a set of sunrise and sunset data examined. An orbit has been selected with an inclination of 70° and an altitude of 600 km. Some relevant data are given in table 1. This choice of orbit altitude and inclination was based on the fact that for moderate altitudes of a few hundred kilometers (to ensure lifetimes of several years), 70° is an inclination which allows coverage at each pole sometime during a year; thus the orbit provides global coverage as defined earlier. (This matter is treated parametrically in the following section.) The orbit was started near the summer solstice of 1981 in an orientation (dependent on the time of day of injection into orbit) which does not produce occultations for the first few days; the initial geometry is shown in figure 3. The orbit so defined is henceforth referred to as the nominal orbit. A mission starting with this initial orbit configuration and lasting for 1 year is referred to as the nominal mission. The launch year is arbitrary and the results could be reproduced for any other year desired.

Figure 4 shows the variation of several important mission parameters as a function of time for 5440 revolutions (1 year) of the nominal orbit. Throughout this figure (and similar figures throughout the paper) the small crosses refer to sunsets, while the dots refer to sunrises. Figure 4(a) shows the variation in the tangent latitude, as previously defined in figure 1, as a

function of time from launch. The cycles of coverage are driven by the orbit precession relative to the Sun and are typical of nonsynchronous orbits. The period of the cycles is about 100 days. This can be verified by noting that the precession rate of this orbit is about -2.5 deg/day relative to inertial space and, consequently, about -3.5 deg/day relative to the Sun. Note that curves in figure 4 are not continuous; they are made up of discrete events occurring at the rate of about 30 per day. The slow change in the northern and southern latitude limits of the coverage is due to the yearly cycle in subsolar declination and some additional orbit constraints. At least the initial distribution of sunrises and sunsets can be understood qualitatively by considering the rotation of the orbit plane from its initial orientation shown in figure 3. For the nominal orbit there are about 9500 measurement opportunities in a year, equally divided between sunrises and sunsets. The exact number is dependent on the precise timing of the launch, which can be altered to shift the coverage cycles within the limits imposed by solar position. It is possible to select a launch time (an initial orbit plane orientation) which will not permit tangent latitude coverage all the way to the poles, so that some planning is necessary in that regard. However, because launch time variations do not have a major effect on the overall performance of a 1-year mission, they are not investigated parametrically in this study.

Figure 4(b) shows, for the nominal mission, the variation in pointing angle β required to track the sunrises and sunsets throughout the year. It is not unexpected that a full $\pm 180^{\circ}$ of scanning is required to accomplish this task. Note the symmetry evident between the sunrise and sunset curves, which may be of considerable significance in setting up a strategy for pointing the spacecraft sensors in preparation for detecting a sunrise based on the angular position of the previous sunset.

The tangent longitude coverage is examined separately for sunrises and sunsets in figures 4(c) and (d), respectively. The overall impression is one of reasonably complete longitude-latitude coverage over a year, but the way in which spatial coverage is built up as a function of time is obscured in these two parts of figure 4. This matter is dealt with in more detail in subsequent figures.

Figures 4(a) to (d) treat all occultation events as equivalent and each tangent point as a single set of two coordinates. In reality, the changing conditions under which these events occur produce variable sunrise and sunset rates which affect the amount of time available for measurements. When the Sun is in the orbital plane, the apparent vertical motion of the Sun's image through the atmosphere is maximum, while at the other extreme, when the spacecraft is moving parallel to the terminator with the Sun off to one side, the sunrise or sunset rate approaches zero. There are potential advantages and drawbacks at each extreme which must be taken into account during mission planning. One way to keep track of these changes is to calculate the vertical motion of the Sun's image relative to the horizon: $v_{rel} = \vec{v}_{SC} \cdot \hat{r}_T$ at the instant when the projection of $\hat{x}_\Theta$ touches the horizon. When the Sun is behind or ahead of the spacecraft, this value is maximum and the length of time required for the Sun's image to pass through the atmosphere is short enough to consider v_{rel} constant during the measurement opportunity. At the other extreme, the motion of the Sun's image in the vicinity of the horizon is more

complicated and must be examined in detail. The cyclic variation between fast and slow sunrises and sunsets is directly related to the yaw angle β, previously identified in figure 4(b). Thus, values of β near 0° or $\pm 180^{\circ}$ place the Sun ahead of or behind the spacecraft and result in fast occultations, while values near $\pm 90^{\circ}$ place the Sun to one side of the spacecraft and result in slow occultations. In figure 4(e), v_{rel} is plotted for the nominal mission. The right ordinate gives the time required for the Sun's image to pass through 100 km of atmosphere at the constant rate v_{rel}. As noted previously, this rate is a good approximation for the larger values of v_{rel}, but becomes less meaningful as the magnitude of v_{rel} approaches zero.

A consequence of the variable measurement time is that the tangent point as previously defined moves during the course of a sunrise or sunset. The resulting smearing of the surface resolution is of concern for interpreting measurements. The correspondence between the time available for measurements and the change in surface coordinates is not a simple one, but the limiting cases can be described. As the spacecraft reaches the extremes of its subsatellite latitude, the change in subsatellite latitude with time is near zero; the rate of change in tangent latitude is also generally lowest if the occultations occur during these portions of the orbit. If the occultations occur when the satellite is near the equator, the rate of change of the subsatellite latitude is maximum, amounting to about $(360^{\circ}/5805 \text{ sec}) \sin 70^{\circ} \approx 0.06$ deg/sec for the nominal orbit. The tangent latitude changes at about the same rate. For the tangent longitude, the situation is reversed, so that the maximum rates of change occur at the highest subsatellite latitudes.

To illustrate the expected changes in surface conditions during a sunrise or sunset, some representative measurement situations have been selected from the nominal mission. It must be emphasized that selecting specific orbit situations for close inspection, as opposed to considering overall mission performance must be viewed with caution. The computer model used to generate occultation data (relative to a spherical surface) is not intended to actually predict the precise occurrence of a particular event many months in advance. Even if a spacecraft were maintained in its orbit so that its actual precession rate exactly matched the approximate values used in this study, there would still be some minor discrepancies in timing of the events because of the difference between the actual Earth horizon and the spherical model of the Earth's surface. These discrepancies would be most noticeable during the slow sunrises or sunsets. However, situations like the ones described in the following paragraph are certain to occur during the course of any similar mission.

A limiting case for a slow sunset and sunrise is examined in detail in figure 5. The upper plot shows the altitude of the center of the Sun's image above the horizon as a function of time (refraction is ignored); the two middle plots show the pointing angles α and β required to track the Sun; and the lower plot shows the latitude and longitude of the tangent point. For this figure, the computer model was temporarily modified to represent the Earth's surface as an ellipsoid (see ref. 4) to improve the estimate of where the horizon actually is. This event is taken from near the beginning of the mission, orbit 107 on day 7. The center of the Sun just reaches the horizon and then starts back up again, giving more than 12 min for observation of the atmosphere below 100 km. On preceding orbits there are other slow passages of the Sun

into and through the atmosphere. Table 2 shows the minimum altitude reached by the Sun on several consecutive orbits and the length of time during which the Sun's center is between the horizon and 100 km. These representative values illustrate the possibilities for measurements near the beginning and end of periods of occultation. Figure 4(e) shows that there are eight occasions during the nominal mission during which the very slow occultations occur, at which time the situations described in figure 5 prevail. Some of the viewing conditions are summarized in table 3 for the slow sunset and sunrise (orbit 107); and they are compared with values for a fast sunset or sunrise taken during the period of maximum relative vertical velocity of the Sun's image with respect to the horizon (orbit 415). The frequency of viewing conditions between the extremes of v_{rel} is given in table 4 by actual count and percentage for the entire nominal mission. As seen in table 4, nearly all of the occultation events occur in less than 100 sec.

To complete specific analysis of the nominal mission, there remains only the additional investigation of tangent longitude-latitude coverage and how it is obtained as a function of time. In figures 6(a), (b), and (c), the tangent longitudes and latitudes of sunrises and sunsets are plotted for the first 7, 30, and 90 days after the start of occultations, respectively. In the first of these plots (7 days) the points associated with the first 15 orbits on which occultations occur are numbered. It is clear from figure 6 that, typically, the 360° range of longitudes is scanned fairly uniformly with a resolution of roughly 25° in a time during which the tangent latitude changes relatively little. A final view of longitude-latitude coverage is presented in figure 7. Here, the Earth's surface has been divided into longitude-latitude boxes of approximately equal area, corresponding to a $5^{\circ} \times 5^{\circ}$ box at the equator, such that the longitude width is an integer factor of 360°. If the latitude band width is fixed, the farther a latitude band is from the equator, the greater must be the longitude span of each box in that band to give the same area. The longitude divisions as a function of latitude are made such that the number of boxes within each 5° latitude band results in the minimum departure of the area of each box from the reference area at the equator ($5^{\circ} \times 5^{\circ} \approx 3 \times 10^{5}$ km^2). A summary of this global division is given in table 5 for one hemisphere. It shows the latitude band, the area included within each band, the number of boxes in the band, the longitude span of each box, the area of each box, the cumulative surface area from equator to pole, the percentage of the hemisphere's area in each band, and the cumulative percentage of hemisphere area from equator to pole. Figure 7 shows that the global distribution of tangent points is not uniform. There is sparse or no coverage of some boxes in the tropics, with heavier coverage toward the poles. (Some parametric examination of this point is presented in the next section.) The lack of uniform temporal coverage, clearly evident in figure 4(a), presents a potential problem in data analysis which is nowhere evident in figure 7. While the ability to obtain point measurements in space and time is potentially valuable, it is of more interest to be able to separate time and space effects and to determine whether the data can be grouped in some way to detect, for example, persistent or permanent spatial differences or trends in some measured quantity over the globe.

Parametric Investigation of Tangent Latitude Coverage Available From Solar Occultation Missions

From the spatial coverage capabilities of a specific hypothetical solar occultation mission, it is of interest to generalize some of the observed results. It is of particular value to understand the factors which influence tangent latitude coverage, as this parameter is the most important one for determining how much of the globe is covered. For any orbit, the available tangent latitudes are constrained to lie within an envelope determined by orbit parameters and solar declination. So, first of all, the boundaries of the envelope must be determined. Figure 8(a) illustrates, for an orbit of inclination i and altitude h, limiting conditions under which a sunrise or sunset can be observed, given a solar declination δ. The spacecraft is at its maximum subsatellite latitude, and the plane of the figure contains $\hat{\varrho}_\Theta$ and $\hat{N}$, as defined in figure 2. Generally, orbits would be oriented so that occultations occur regularly as the spacecraft passes into and out of the Earth's shadow. However, for some conditions, as illustrated in figure 8(a), it is possible for a spacecraft to be in continuous sunlight. The limiting case[1] occurs when

$$D + i + |\delta_\Theta| = 90^\circ \tag{2}$$

where D is the Earth central angle between spacecraft and tangent point at the horizon:

$$D = \cos^{-1}\left(\frac{r_\oplus}{r_\oplus + h}\right) \tag{3}$$

The angle D is a constant of the orbit, a function only of the circular orbit altitude h. For the conditions shown, sunrises and sunsets occur just at the northern extreme of the terminator latitude. (There is an analogous geometry for the southern extreme, when δ_Θ is negative.) Such occultations occur, in the limit, at $\lambda_T = 90^\circ - |\delta_\Theta|$. Note that this is a limit imposed by the latitude extremes of the solar terminator. Additional constraints may be imposed by the ability of a spacecraft to view occultations at any particular time; that is, the spacecraft must be able to view the terminator from the dark side, looking perpendicular to the terminator from an angular distance D. If h or i is increased or if δ_Θ is decreased, in figure 8(a), no occultations could be observed for this orientation of the orbit plane.

---

[1] If $i > 90^\circ$ (as for Sun-synchronous orbits), use $180^\circ - i$ in place of i for these calculations.

Then,

$$
\left.
\begin{aligned}
\sin B &= \frac{\tan D}{\tan d} \\
\cos d &= -\cos i \cos \eta + \sin i \sin \eta \cos c \\
\frac{\sin b}{\sin i} &= \frac{\sin c}{\sin d} \\
\sin b &= \frac{\sin c \sin i}{\sin d} \\
\sin \lambda_T &= \begin{cases} \sin (b + B) \sin (180^\circ - \eta) = \sin (b + B) \sin \eta & \text{(Northern Hemisphere)} \\ \sin (b + 180^\circ + B) \sin (180^\circ - \eta) = -\sin (b + B) \sin \eta & \text{(Southern Hemisphere)} \end{cases}
\end{aligned}
\right\} \quad (6)
$$

Note that when $|\tan D/\tan d| > 1$, $|\sin B| > 1$ and no occultations can occur. These equations hold only for $i \leq 90^\circ$. The angle c defines the nodal orientation of the orbit relative to the solar terminator. For the purposes of plotting data from equation (6), it is more convenient to use nodal orientations relative to the subsolar meridian $\Omega - RA_\odot$. Varying c from -270° to $+90^\circ$ is equivalent to varying the quantity $\Omega - RA_\odot$ from -180° to $+180^\circ$.

In figure 11, the variation of tangent latitude with nodal orientation relative to the subsolar meridian is shown for 600-km circular orbits having inclinations of 50° and 70°, with solar declination as a parameter. Figure 11(a) shows this variation for the 50° orbit with solar declinations of 0°, $\pm 16^\circ.1$, and $\pm 23^\circ.44$. At each value of $\Omega - RA_\odot$ the limiting northern and southern tangent latitudes are shown with $\delta_\odot$ as a parameter. The choice of $\delta_\odot = \pm 16^\circ.1$ is not arbitrary; it is the limiting declination for which periods of continuous sunlight are possible with this orbit. For $|\delta_\odot| > 16^\circ.1$, there are orbit plane orientations which produce no occultations. It is clear from figure 11(a) that limiting declinations of $\pm 16^\circ.1$ produce the maximum limits on tangent latitudes for this orbit. The fact that the maximum magnitude of the tangent latitude occurs at some time other than when the terminator passes through the poles may appear contradictory, as the equinoxes mark the only times at which pole-to-pole coverage is possible under any orbit conditions. Qualitatively, this result may be explained by noting that the poles are never visible from the 50°, 600-km orbit, and occultations can only occur at visible latitudes where the spacecraft can view the sun perpendicularly across the terminator.

In figure 11(b), available tangent latitudes are shown for a 70°, 600-km orbit. Here, continuous sunlight can occur at any solar declination for some

angular orientation of the orbit plane. Also, polar coverage is available from this orbit when the terminator goes through the poles (i.e., when $\delta_\odot = 0^\circ$). The solar declinations of $\pm 10^\circ$ have no special significance for this orbit and are just intermediate values to illustrate the tangent latitude behavior.

As an example, consider the envelope of available tangent latitudes for the 50°, 600-km orbit as a function of solar declination. Minimum and maximum values of λ_T are available from figure 11, for the orbits and solar declinations considered there, with equation (6) available to fill in additional points as needed. In principle, the analytic derivative of equation (6) with respect to c or some trigonometric function of c could be set equal to zero and evaluated with the required orbital parameters, but such an analytic solution has not been found. The maximum magnitude of tangent latitude $|\lambda_T|$ as a function of solar declination is illustrated in figure 12 for the 50°, 600-km orbit. One boundary on the latitude is formed by the solar terminator itself, while the other is formed by orbital constraints. Note that the maximum latitude magnitude of $73^\circ.9$ is reached when $|\delta_\odot| = 16^\circ.1$, and this occurrence also marks the boundaries between which periods of continuous sunlight are possible. As indicated on the figure, $|\delta_\odot| \geq 16^\circ.1$ between May and August and again between November and February.

Figure 13 shows the envelopes of available tangent latitudes for several 600-km circular orbits which result from consideration of solar declination and of figure 11 in the case of the 50° and 70° orbits and similar calculations for the other orbits. The abscissa is linear with time, rather than with solar declination, so the resulting envelope could be superimposed on plots of actual or simulated tangent latitude variations such as figure 4(a). Table 6 (adapted from ref. 3) gives a tabulation of solar declination and right ascension as a function of time from January 1 and the vernal equinox, from which the terminator restrictions can be obtained for figure 13. Clearly, all the points north of the terminator curve in the Northern Hemisphere or south of terminator curve in the Southern Hemisphere are inaccessible with any orbit orientation. Any additional constraints on the envelope are due to the orbit. As previously noted for the 50°, 600-km orbit, the maximum northern or southern tangent latitudes occur not at the equinoxes, when the terminator goes through the poles, but between the times of the equinoxes and solstices. The maximum available latitude of $73^\circ.9$, north or south, for the 50° orbit is equal to 90° minus the minimum solar declination which allows some periods of continuous sunlight. Note that in figures 12 and 13 the envelopes are not smooth curves; the orbit constraint curve intersects the solar declination constraint rather than blending in with it.

Also shown in figure 13 is the envelope for a 60°, 600-km orbit, which has a maximum available tangent latitude of $83^\circ.9$, and a 40°, 600-km orbit which should never reach the solar declination limit according to figure 9. The envelope for a 70°, 600-km orbit follows the solar terminator curve during each hemisphere's summer season. This is to be expected from figure 9, which indicates that at 600 km, any inclination above $66^\circ.1$ ($90^\circ - 23^\circ.9$) allows periods of continuous sunlight regardless of solar declination. This is equivalent to saying that such an orbit can always be oriented so that the Sun may be viewed across the terminator at either its northern or southern limits (but not both at the same time of year).

Finally, the maximum tangent latitudes, north or south, which are available from various orbits are summarized in table 7. These data are just extensions of the calculations for figure 9. Also given in the right column of table 7 is the minimum inclination which allows polar coverage at the equinoxes as a function of circular orbit altitude; these data are also based on the calculations used for figure 9 and are included here for completeness.

It can be seen now that mission-particular solar occultation data such as those found in figure 4 can be generalized with the help of the preceding discussion. The tangent latitudes vary within boundaries which are not visible in figure 4, and these can be specified for any required orbit, as in figure 13, so that at least the limiting effects of varying launch conditions can be assessed. These effects include a seasonal component due to the Sun's motion in declination and a daily component, equivalent to varying the nodal relationship of the orbit to the Sun. Information such as that contained in figure 11 is directly applicable to determining the details of measurement opportunities available during a given part of the year. If periods of continuous sunlight are of interest, for either their deliberate inclusion or exclusion, figures 9 and 11, or their equivalents for particular orbits of interest, provide the necessary mission-planning data. The geographical distribution of measurements can be tailored to some extent by choosing the season and time of day of launch. This is especially important for short-term missions, as orbital precession is too slow to yield in a few days the variety of measurement opportunities available over the space of a year.

To illustrate how tangent latitudes vary within the boundaries defined in figure 13, figure 14 illustrates tangent latitudes for a 50°, 600-km orbit. In figure 14(a) the initial nodal orientation relative to the Sun is the same as for the nominal mission. In 14(b) the orbit plane is rotated by 90° to produce sunrises and sunsets at the start of the mission instead of after a period of continuous sunlight. The tangent latitude envelope for this orbit, from figure 13, is superimposed on each part of figure 14; the periods during which continuous sunlight is possible are also shown. As expected, the resulting cycles of tangent latitude for each initial condition are contained within the envelope, and periods of no occultation are restricted to those times of the year when the magnitude of the Sun's declination exceeds 16°.1. Note the faster cycles of tangent latitude for the 50° orbit relative to the 70° nominal orbit. From reference 3, the nodal precession rate is proportional to cos i:

$$\dot{\Omega} \approx \frac{-2.0646 \times 10^{14} \cos i}{a^{3.5}} \text{ deg/day} \qquad (7)$$

Table 8 gives nodal precession rates for a variety of orbits. Note that $\dot{\Omega}$ is zero at an inclination of 90° and positive for angles greater than 90°. Inclinations of around 100° are in the range of Sun-synchronous orbits, for which $\dot{\Omega}$ needs to be 0.9856473 deg/day (see ref. 3). A conflict is clearly evident between frequency of coverage at some latitudes, driven by the nodal precession rate, and total portion of the globe covered, a function of orbit inclination and altitude. For example, equatorial latitudes are covered on 23 occasions

during 1 year from a 50°, 600-km orbit, but there is no polar coverage. To achieve this at the same altitude, a higher inclination is required and for the 70° nominal mission, equatorial coverage is reduced to 15 occasions per year.

A final item of parametric interest relative to figure 14 is the distribution of measurements as a function of latitude. It is clear from figures 4(a), (c), and (d) that there are many more measurements at some latitudes than at others. Distributions of number of measurements as a function of tangent latitude, in 5° bands, are shown in figure 15 for 1-year missions with 600-km orbits having inclinations of 70°, 60°, and 50°. The peaks in the northern and southern latitudes, away from the equator, are typical of many kinds of Earth-pointing measurements made from space. The lack of complete symmetry about the equator is due to having picked a particular initial orbital relationship to the Sun, the effects of which are not overridden in a 1-year mission. The initial nodal orientation for all three orbits in figure 15 is the same as that used for the nominal mission of figure 4. The data for the 70° orbit may be obtained directly from figure 7 by summing all the "boxes" in each 5° latitude band. The total number of measurements resulting from a 1-year mission increases as the inclination decreases, as the total length of all periods of continuous sunlight decreases with decreasing i (due to the more rapid orbit plane precession rate). Of course, the total number of occultation opportunities is limited to twice the number of orbits, a value achieved when no periods of continuous sunlight are possible.

In addition to considerations of coverage on the Earth's surface, through the tangent points and their projections through the atmosphere, there is also some potential interest in what is viewed on the surface of the Sun. For example, what are the heliographic (Sun-centered) coordinates of the unit vector $\hat{x}_\Theta$ which has been used in the previous mission analyses for defining Sun viewing conditions? If the Sun's disk is scanned from edge to edge, what are the heliographic coordinates available to the viewer? This may be of concern in avoiding or accounting for sunspot activity, which is known to be a function of heliographic latitude (see ref. 5, for example). For instruments whose field of view is small compared with the angular size of the Sun (approximately 0.5 deg) it is also possible that accurate instrument calibrations and data interpretation may be compromised if the viewing conditions on the Sun are not well known during the time of calibration and data taking. Such information can be generated during preliminary mission analyses by making use of information calculated at the time of occultation. The problem is complicated geometrically by the Sun's rotational axis not being perpendicular to the ecliptic; that is, its equator does not lie in the ecliptic. Earth-centered vectors must first be transformed into a heliocentric-ecliptic system and then into the heliographic system, or vice versa. Because of the peripheral nature of this problem, its self-contained solution is dealt with in appendix B. An example is given there of how the heliographic coordinates might change over the year during the nominal mission.

STATISTICAL INTERPRETATION OF DATA FROM SOLAR OCCULTATION MISSIONS

In order to understand how data from long-term solar occultation missions may be interpreted, it is necessary to augment the information already generated

for the simulated missions described previously. The spatial and temporal distributions of measurement opportunities have already been specified for the nominal mission of figure 4 (70° inclination, 600-km altitude, 1 year). In keeping with the general approach outlined in the introduction to the paper, a single additional "output" quantity q is now associated with each measurement opportunity. For the nominal mission there are 9480 such opportunities. The parameter q is a function of tangent longitude, tangent latitude, and time. It is assumed for the present purposes to have been obtained directly without measurement error, even though the process of obtaining values of q as a result of an actual mission may well be an arduous and error-prone task. The physical variable which q represents is assumed to have both systematic and random variability. No other physical characteristics need be attributed to q. A dimensionless numerical value is assigned to each sunrise or sunset measurement opportunity, uniquely specified by its time and position coordinates. The mathematical model which produced the simulated measurements is not given except as it can be determined from the measurements themselves. This approach is an attempt to free the discussion which follows from the prejudice of additional knowledge which may not exist for a real mission.

The problem of data interpretation is to group the measurements in a meaningful way and to search these groupings for patterns which emerge. It is of interest here to produce a function which shows how q, or its average, varies as a function of time. Figure 4(a) shows that the tangent point passes through a particular latitude several times per year, depending on the latitude. This occurs on 15 different occasions per year at equatorial latitudes (for the nominal mission), but only once or twice at polar latitudes. Additionally, figure 6 has shown that complete longitudinal coverage is obtained at about 25° intervals, during a period of time (a little over a day) in which the tangent latitude changes very little. Thus, figures 4(a) and 6 can be used to justify grouping solar occultation data in subsets corresponding to measurements taken during small time intervals, within bands of latitude. Longitudinal dependence may be removed if it can be assumed to be negligible, or to be properly averaged by considering the available data within a band of latitude. In fact, for many measurements of interest, dispersion and transport of atmospheric constituents is much more rapid to the east and west than it is to the north and south, leading to longitudinal uniformity when no comparable uniformity exists as a function of latitude. In any event, it is necessary to quantify this assumption. Let $\bar{t}$ be an average time during which a subset of measurements is made, and let $\bar{\lambda}$ be the midpoint in a latitude band (5° bands are used for this study):

$$\left.\begin{aligned} \bar{t} &= \frac{t_{last} + t_{first}}{2} \\ \bar{\lambda} &= \frac{\lambda_{high} + \lambda_{low}}{2} \end{aligned}\right\} \tag{8}$$

Within each latitude band and time interval, there exists a true mean μ_q:

$$\mu_q(\lambda,t)\Big|_{\bar{\lambda},\bar{t}} = \frac{1}{2\pi}\frac{1}{\Delta t}\frac{1}{\Delta\lambda}\int_0^{2\pi}\int_{\Delta t}\int_{\Delta\lambda} q(\lambda,L,t)\, d\lambda\, dt\, dL \tag{9}$$

It is assumed that for n_q measurements of some parameter q within a particular latitude band, the true mean can be approximated as a function of latitude and time by

$$\bar{q}(\lambda,t)\Big|_{\bar{\lambda},\bar{t}} = \frac{\sum_{i=1}^{n_q} q_i(\lambda,L,t)}{n_q} \tag{10}$$

Table 9 gives a set of values of $\bar{q}(\bar{\lambda},\bar{t})$ for the nominal mission. Within each 5^o latitude band, starting at the South Pole, measurements are grouped according to time in the following way: if a measurement time differs from the preceding one by less than a day, it is retained in the current data subset; otherwise a new subset is started. This procedure groups the data in the natural way indicated by figure 4(a). Near the equator there are 15 such subsets in a year. Table 9 lists for each subset (there are from 1 to 15 subsets in each latitude band) the number of measurements n_q, the mean value $\bar{q}$, the sample standard deviation s_q, the average time of the measurement $\bar{t}$, and the first and last measurement time t_{first} and t_{last} referenced to the beginning of a calendar year, January 1, 1981. It has been assumed for simplicity of presentation that the data are periodic over a year so that information obtained on any date is the same except for random components as that obtained on the same date in adjacent years. Hence the data obtained in 1982 can be used to fill in the 1981 data prior to the mission launch time. This need not apply to an actual mission, but no difficulty is introduced into the analysis if such an assumption is not made. The sample variance s_q^2 is computed in the usual way:

$$s_q^2 = \frac{\sum_{i=1}^{n_q}(q_i - \bar{q})^2}{n_q - 1} = \frac{\sum_{i=1}^{n_q} q_i^2 - \left(\sum_{i=1}^{n_q} q_i\right)^2 \Big/ n_q}{n_q - 1} \tag{11}$$

For those cases where $n_q = 1$, s_q is not defined, and such places are noted by blanks in table 9; the first and last measurement times are also left blank.

There are still uncertainties to be resolved about each $\bar{q}$ and its relationship to the true mean μ_q over the same time interval. In general, the distribution of various atmospheric constituents represented here by q may be driven by diurnal and short-term cycles in addition to a longer term (seasonal) cycle whose behavior is sought as a result of the proposed 1-year nominal mission. It is clear that diurnal cycles are fundamentally inaccessible through solar occultation measurements, which are restricted to local dawn or dusk conditions. The short-term cycles might be driven in longitude by what are commonly known as planetary waves (which may also exhibit long-term patterns), and their behavior might typically be of considerable interest in an actual mission. The sampling frequency of q (about 30 per day) or, equivalently, the longitudinal spatial resolution of about 25° (recall fig. 6) poses certain problems for extracting short-term temporal information from this type of mission. Detailed consideration of these matters is beyond the scope of this paper. Note that the span of time over which each $\bar{q}$ is formed, $t_{last} - t_{first}$, is short compared with the seasonal cycle of interest and it is assumed that the behavior of the short-term cycles is such that $\bar{q}$ is equal to the true mean as defined in equation (9). If this assumption breaks down because of planetary wave behavior, other short-term behavior, or more permanent longitudinal nonuniformities, then a one-dimensional spatial concept of latitude zonal averages over the time scales of interest would not be valid and should be discarded in favor of a two-dimensional spatial grid. These questions deserve closer scrutiny when measurements are considered for atmospheric constituents whose actual behavior is known to some extent, either from theory or previous measurements. In particular, the restriction of solar occultation measurements to dawn and dusk means that some understanding of diurnal behavior is essential for proper interpretation of the $\bar{q}$'s.

Suppose now that it is desired to determine a yearly mean $\mu_{\bar{q}}$ as a function of latitude:

$$\mu_{\bar{q}}(\lambda)\Big|_{\bar{\lambda}} = \frac{1}{2\pi}\,\frac{1}{365}\,\frac{1}{\Delta\lambda}\int_0^{2\pi}\int_0^{365}\int_{\Delta\lambda} q(\lambda,L,t)\; d\lambda\; dt\; dL \qquad (12)$$

It is certain that $\mu_{\bar{q}}$ cannot be obtained just by taking the unweighted mean of all the q's in each latitude band. The difficulty with such a procedure is easily seen by referring to the column labeled n_q in table 9. For example, in the latitude band from -65° to -60°, n_q varies from 5 to 218, so that an unweighted average of all the q's in this band favors some measurement opportunities over others when there is no reason to do so. This difficulty is found in all the latitude bands, so taking unweighted averages is clearly not an acceptable use of the available data. Another approach is to use the $\bar{q}$'s themselves as data and average them to estimate $\mu_{\bar{q}}$. This could be thought of as a way of weighting the individual points within each subset of measurement opportunities. It is an intuitively attractive way to achieve the desired results, especially when there appear to be "enough" values of $\bar{q}$. If the $\bar{q}$'s are used in this way, it is then tempting to say, as in equation (10), that for each latitude band the yearly average $\mu_{\bar{q}}$ is estimated by a quantity $\bar{Q}$:

$$\bar{Q}(\lambda)\Big|_{\bar{\lambda}} = \frac{\sum_{i=1}^{n_{\bar{q}}} \bar{q}_i}{n_{\bar{q}}} \tag{13}$$

where $n_{\bar{q}}$ is the number of data subsets for each latitude band in table 9. If this is an acceptable procedure, then the variance is

$$s_{\bar{q}}^2 = \frac{\sum_{i=1}^{n_{\bar{q}}} \bar{q}_i^2 - \left(\sum_{i=1}^{n_{\bar{q}}} \bar{q}_i\right)^2 \Big/ n_{\bar{q}}}{n_{\bar{q}} - 1} \tag{14}$$

However, it is a fundamental characteristic of the solar occultation technique that such calculations are not justified in the statistical sense. Equations (13) and (14) presume that the samples (the $\bar{q}$'s) are taken uniformly (in time) from the total population. The distribution of $\bar{q}$ appears uniform near the equator but is clearly not uniform near the poles. At intermediate latitudes the distribution is difficult to assess in a strictly quantitative way. Because of the problems with applying otherwise straightforward descriptive statistics, no statistically acceptable confidence limits can be placed on $\bar{Q}$ as calculated with equation (13). That is, it is not necessarily true that there is a 95-percent probability that the true mean $\mu_{\bar{q}}$ differs from $\bar{Q}$ by no more than $\pm 2s_{\bar{q}}$, as would be the case if the $\bar{q}$'s were normally distributed. The well-known t-statistic, which might be used for establishing confidence limits when the population variance is not known, is not applicable either, as it, too, requires that the samples from the population be randomly selected.

An alternative way to arrive at the desired goal of establishing a yearly mean within a latitude band is to propose a model for describing the behavior of $\bar{q}$. At the center of each latitude band let

$$\bar{q} = Q + A \sin(360t + \gamma) + \varepsilon \tag{15}$$

where Q is the mean value of $\bar{q}$ averaged over a year, A is an amplitude, t is time in fractions of a year, γ is a phase factor (in degrees), and ε is a residual term. This is a very simple periodic model which, through γ, allows some adjustment of the location of the maximum and minimum values within the yearly cycle. The residual term can incorporate random error as well as unmodeled variability. Equation (15) can be rewritten as follows:

$$\bar{q} = \mathcal{Q} + A \cos\gamma \sin 360t + A \sin\gamma \cos 360t + \varepsilon \tag{16}$$

Or, letting $C_1 = \mathcal{Q}$, $C_2 = A \cos\gamma$, and $C_3 = A \sin\gamma$,

$$\bar{q} = C_1 + C_2 \sin 360t + C_3 \cos 360t + \varepsilon \tag{17}$$

For n measurements of $\bar{q}$, $M_1, \ldots, M_i, \ldots, M_n$:

$$\begin{bmatrix} M_1 \\ \cdot \\ \cdot \\ \cdot \\ M_i \\ \cdot \\ \cdot \\ \cdot \\ M_n \end{bmatrix} = \begin{bmatrix} 1 & \sin 360t_1 & \cos 360t_1 \\ \cdot & \cdot & \cdot \\ \cdot & \cdot & \cdot \\ \cdot & \cdot & \cdot \\ 1 & \sin 360t_i & \cos 360t_i \\ \cdot & \cdot & \cdot \\ \cdot & \cdot & \cdot \\ \cdot & \cdot & \cdot \\ 1 & \sin 360t_n & \cos 360t_n \end{bmatrix} \begin{bmatrix} C_1 \\ C_2 \\ C_3 \end{bmatrix} + \begin{bmatrix} \varepsilon_1 \\ \cdot \\ \cdot \\ \cdot \\ \varepsilon_i \\ \cdot \\ \cdot \\ \cdot \\ \varepsilon_n \end{bmatrix} \tag{18}$$

In matrix notation,

$$\underline{M} = \underline{B}\underline{C} + \underline{\varepsilon} \tag{19}$$

where $\underline{C}$ is a 3×1 matrix of parameters to be estimated and $\underline{B}$ is a $3 \times n$ matrix of coefficients evaluated at the measurement times $t_1, \ldots, t_i, \ldots, t_n$. It is then well known that the set of parameters which minimizes the sum of the squares of the residuals (the unweighted least squares estimate) is given by

$$\hat{\underline{C}} = (\underline{B}^T\underline{B})^{-1}\underline{B}^T\underline{M} \tag{20}$$

From the elements of $\hat{\underline{C}}$ ($\hat{C}_1$, $\hat{C}_2$, and $\hat{C}_3$) the desired model parameters are

$$\left.\begin{aligned} \hat{\mathcal{Q}} &= \hat{C}_1 \\ \hat{\gamma} &= \tan^{-1}\left(\hat{C}_3/\hat{C}_2\right) \\ \hat{A} &= \hat{C}_2/\cos\hat{\gamma} \end{aligned}\right\} \tag{21}$$

Recall that the problem with calculating statistical means, as in equation (13), was one of interpreting the results. Now, with a model and its parameters, this interpretation is made straightforward in its own restricted way. In the least squares sense described above, the model parameters in table 10 are the best ones obtainable for the model used. It remains only to calculate how much of the observed variability in the data (the $\bar{q}$'s) is represented by the model. With three parameters, three data points can be represented perfectly, while more than three are generally imperfectly represented. This may be true even if the postulated model is the true model, because of the possible existence of random error in the data. It can be shown that for any observed value Y_i from a set of observed values, its expected value $\hat{Y}_i$ (as calculated from a model), and the mean value $\bar{Y}$ of all observed values in the set, the following relation holds:

$$\sum_i (Y_i - \bar{Y})^2 = \sum_i (\hat{Y}_i - \bar{Y})^2 + \sum_i (Y_i - \hat{Y}_i)^2 \qquad (22)$$

Sum of squares about the mean = Sum of squares due to regression + Sum of squares about the regression

This well-known statistical result expresses the fact that the variability about the mean (the sum of squares about the mean) is explainable in terms of the modeled variability (the sum of squares due to regression) plus the unmodeled variability (the sum of squares about the regression). It is desired that the unmodeled variability be small, that is, that the ratio

$$R = \frac{\sum_i (\hat{Y}_i - \bar{Y})^2}{\sum_i (Y_i - \bar{Y})^2} \qquad (23)$$

be close to unity. If R is 1 (or 100 percent), then the model perfectly represents the data. If R is less than 1, then there is variability which has not been accounted for with the existing model; this may be random or systematic variability.

The last column of table 10 shows R for the least squares fit to each applicable latitude band. It is interesting to note that almost none of the variability in the data is represented by the model near the equator. This corresponds to the decreasing amplitude of the sine curve, A, near the equator; there is very little systematic variability of the form postulated. It is tempting to conclude that the variability which is seen near the equator is only random variation in $\bar{q}$, but this conclusion, based on the information presented here, is unwarranted; it can be said only that the postulated model

does not work everywhere. Farther away from the equator, the model appears to do better, indicating the possible existence at these latitudes of a marked annual cycle of simple (sinusoidal) structure. This model seems at least conceptually to have obtained a result, the yearly average value $\hat{Q}$, which was not obtainable with the simple descriptive statistics described previously. It could be argued that even better results could be obtained with a more sophisticated model. However, there are some basic problems with the present approach which are analogous to the lack of confidence in computed statistical means. The least squares technique guarantees, in a particular sense, the best values for the model coefficients, given a particular set of data. But, the goal of modeling is not just to represent one set of data, but to represent the functional behavior of the quantity of interest. If the same model were applied to other samples of $\bar{q}$, different coefficients would result. In fact, if several sets of $\bar{q}$'s are used, all of which are uniformly distributed over a year within each latitude band, the resulting coefficients can be shown to be normally distributed with variances related (through a measure of the error variance) to the diagonal components of the matrix $(B^TB)^{-1}$ as defined in equation (20). These variances are largest when $n_{\bar{q}}$ is smallest. When $n_{\bar{q}} = 3$, the data are represented perfectly by the model, but the variances associated with the coefficients are no longer defined. This means, for example, that the behavior of $\bar{q}$ cannot be predicted anywhere else within that latitude band. Closer to the equator, the variances are smaller, and hence the model has more usefulness as an interpolative tool. The coefficients can be assumed to be correct and the residual term can be assumed to represent random components with variance s_R^2, where s_R^2 is the sum of squares of the residuals based on three degrees of freedom (because three parameters have been calculated):

$$s_R^2 = \frac{\sum_{i=1}^{n_{\bar{q}}} (\bar{q}_i - \hat{\bar{q}}_i)^2}{n_{\bar{q}} - 3} \tag{24}$$

The estimated value of $\bar{q}_i$, $\hat{\bar{q}}_i$, is obtained from equation (15) using the coefficients from equation (21). Despite the difficulty of using the model coefficients with s_R^2 to predict a range for the values of $\bar{q}$, s_R^2 is given in table 10 for each latitude band having enough data; the values tend to be largest near the equator, but there is no explanation for this behavior within the information presented.

There are two reasons for not calculating the coefficient variances in this paper. First, the samples of $\bar{q}$ are not demonstrably uniformly distributed in all cases, especially near the poles. Second, the error variance associated with the $\bar{q}$'s is not known. It may be related to s_R^2, which would be the variance due to random components in $\bar{q}$ if the postulated model were the true model and the residual represented only random contributions to $\bar{q}$ due to the properties of the physical parameter represented by $\bar{q}$. (It may be believed that the distribution of any quantity in the atmosphere is ultimately deterministic, but the time scale of the driving processes may be

such that the results would appear truly random when superimposed on the occultation measurements.) It is more likely that the model is too simple, incomplete, or wrong, and that the error variance should be some composite of variances of the q's (the original data) as determined from equation (11). That is, there should be some global function which determines the size of the random components superimposed on $\bar{q}$. A measure of the true error variance is rarely possible; it requires repetition of measurements in both space and time. This is fundamentally unattainable with satellite measurements and requires, as a minimum, the assumption that equivalent future times can be found to substitute for repetitive measurements at the same time.

As a final comment on the use of models to represent satellite data, note that the success of such models in representing data no more guarantees their physical correctness than a lack of such success indicates their unsuitability. In the present example, data have been represented very well over part of the globe (near the poles), but the data themselves are insufficient for qualitatively satisfying explanations of parametric behavior. In other regions, common sense seems to dictate that explanations in terms of small systematic variability and large random components are reasonable in spite of a lack of statistical rigor in the arguments. Further definition of this situation demands additional insight from theory and experiment as well as ample justification for detailed analysis.

CONCLUDING REMARKS

In the first part of this paper, the orbit dynamics of solar occultation have been discussed first for a particular mission and then in a more general way. This order of presentation uses a hypothetical mission to define important characteristics of all solar occultation missions so that the most significant points can be amplified in the parametric discussions. Observability of the Sun from space as it rises or sets on the horizon is determined by orbit parameters and seasonal factors; the interdependence between satellite and Sun is a complicated one, as both source and observer contribute to a constantly changing geometry. Emphasis has been placed on understanding the distribution of measurement opportunities over the surface of the Earth. The critical spatial coordinate is latitude. Good longitude coverage is guaranteed by the Earth's rotation, at a much higher rate (1 revolution per day) than the rotation of the orbit plane in inertial space (a few degrees per day). Pole-to-pole latitude coverage is available only in the spring and fall, when the solar terminator passes through the poles. Even then, orbit parameters - altitude, inclination, and orbit plane orientation - may prohibit coverage at the northern and southern latitude extremes. A year-long nominal mission (70° inclination, 600-km altitude) has been chosen to provide coverage which extends into both polar regions in the spring and fall. Solar occultation latitude coverage patterns are characterized by their cyclic behavior, driven by precession of the orbit plane and the Sun's motion in inertial space. At some higher inclinations and latitudes, periods of no occultation can occur, during which the Sun is always in sight of the spacecraft. These periods typically last a few days. A special case occurs for Sun-synchronous orbits, where the precession rate matches the average angular rate of the Sun (about 1 deg/day). Then the initial geometry is maintained, on the average, and geographical coverage is

limited in latitude or nonexistent if the geometry is such that no sunrises or sunsets may be viewed.

Temporal coverage is characterized most prominently by its restriction to local dawn or dusk. With 2 measurement opportunities per orbit, there can be on the order of 10^4 measurements during a year. The uneven seasonal distribution of the measurements (within bands of latitude, for example) is such that straightforward statistical interpretation of time-averaged quantities of interest is not possible. This problem has led to the second major division of the paper, in which some statistical limitations of solar occultation data are discussed in detail. The procedure involves the association of a single output quantity with each measurement opportunity. All that is known about this quantity, for the purposes of this paper, is that substantial variability is revealed by the available data. Although there are certain qualitatively "obvious" conclusions which can be drawn from an examination of the data, the nature of the data prevents statistically meaningful confidence limits from being placed on some apparently simple calculations. If descriptive statistics are discarded in favor of mathematically modeling the functional behavior of the observed quantity, it is shown that the extent to which variability of a particular finite set of data can be represented in a mathematical way has little to do with the physical appropriateness of the model. (The simple model proposed represents the data quite well over some portions of the globe, but there is no reason whatsoever to embrace its physical implications.) If it is realized that functional representation of certain behavior is the goal of modeling, and not just the representation of a specific set of data, it has been concluded that statistical confidence in the modeling coefficients may be as lacking as confidence limits were for averaged quantities in the descriptive statistics. The persistent interpretive problems with these data are reassuring in a way, because they arise from insufficient information about the quantity of interest; any technique would be suspect if it appeared to overcome such difficulties in the absence of additional information, either actual or assumed.

This paper shows that long-term solar occultation missions can contribute significantly to understanding the Earth's atmosphere. In some cases, when measurements obtained in this way will be the only ones available, their statistical adequacy is of secondary importance. For valid statistical analyses to be applied to global descriptions of parametric behavior, such measurements must eventually be supplemented with other sources of information. Similar approaches can be applied to occultation involving objects other than the Sun, natural or man-made. The caveats encountered in data analysis are applicable, as well, to other environmental measurements; they point to the need for careful experiment design whenever such control can be exercised.

Langley Research Center
National Aeronautics and Space Administration
Hampton, VA 23665
January 10, 1980

APPENDIX A

DETERMINING THE CONDITIONS UNDER WHICH THE SUN IS OCCULTED BY THE EARTH RELATIVE TO A SATELLITE HAVING FIXED ORBIT ELEMENTS

Solution of the occultation problem involves determining the points on its orbit at which a satellite enters or leaves the Earth's shadow. The geometry is shown in sketch (A1). The symbols used for this appendix form a

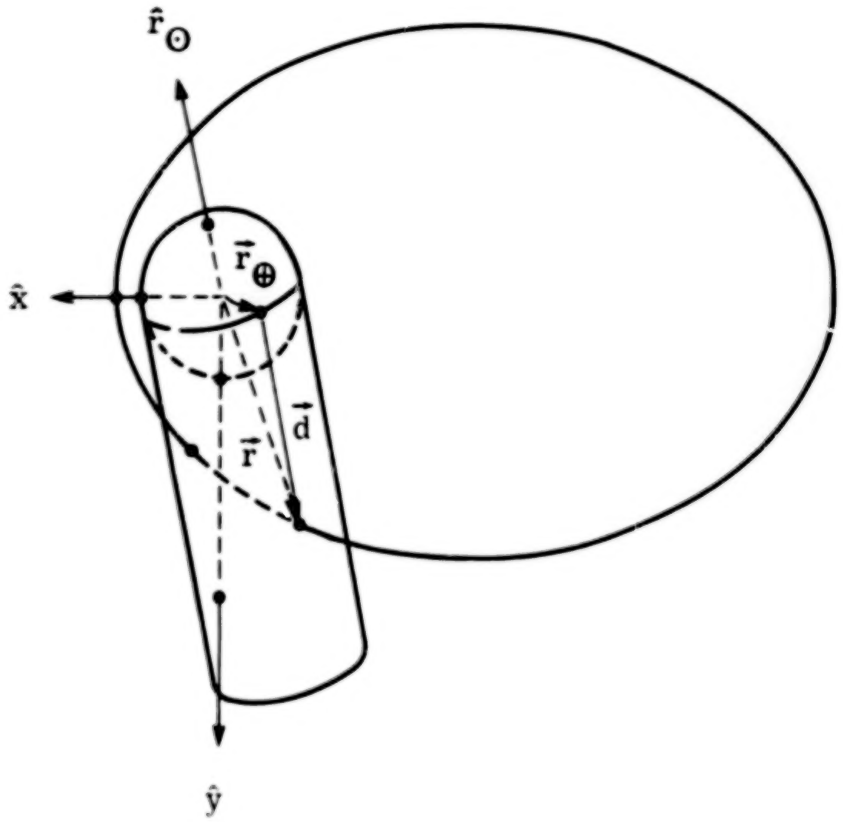

Sketch (A1)

self-contained set, and they are not all defined in or consistent with the symbol lists in the body of the paper or in appendix B. All the vector quantities are expressed in a system whose x-y plane lies in the plane of the satellite orbit, with $\hat{x}$ and $\hat{y}$ oriented as indicated in sketch (A1). Such a coordinate system is called the PQW system. Vectors can be rotated into the PQW system by standard procedures. (See, for example, ref. 6.)

A_0 to A_4 constants as defined below

$\vec{d}$ vector perpendicular to the terminator, extending from the terminator to the satellite, km

e eccentricity

f true anomaly, deg

p semilatus rectum, km

$\vec{r}$ radius vector to satellite, km

$\hat{r}_\odot$ unit vector to the Sun

$\vec{r}_\oplus$ Earth radius vector to the terminator, km

$\hat{x}$ unit vector in direction of the perigee of the satellite orbit

$\hat{y}$ unit vector at right angles to $\hat{x}$ along the semilatus rectum

ψ angle between $\hat{r}_\odot$ and $\vec{r}$, deg

The geometric constraint is the requirement that at a point where the satellite enters or leaves the Earth's shadow,

$$\hat{r}_\odot \cdot \vec{d} = -d = -(r^2 - r_\oplus^2)^{1/2} = r \cos \psi$$

That is, $\hat{r}_\odot$ and $\vec{d}$ are antiparallel. This restriction can be written in another way:

$$\hat{r}_\odot \cdot \vec{d} = \hat{r}_\odot \cdot (\vec{r} - \vec{r}_\oplus) = \hat{r}_\odot \cdot \vec{r} = r\hat{r}_\odot \cdot (\hat{x} \cos f + \hat{y} \sin f) = r \cos \psi$$

The x- and y-components of the unit vector to the Sun are

$$r_{\odot x} = \hat{r}_\odot \cdot \hat{x}$$

$$r_{\odot y} = \hat{r}_\odot \cdot \hat{y}$$

Then,

$$r_{\odot x} \cos f + r_{\odot y} \sin f = - \frac{(r^2 - r_\oplus^2)^{1/2}}{r}$$

Since $r = p/(1 + e \cos f)$,

$$\frac{p}{1 + e \cos f}(r_{\odot x} \cos f + r_{\odot y} \sin f) + \left[\frac{p^2}{(1 + e \cos f)^2} - r_\oplus^2\right]^{1/2} = 0$$

This can be rewritten in terms of $\cos f$:

$$A_0 \cos^4 f + A_1 \cos^3 f + A_2 \cos^2 f + A_3 \cos f + A_4 = 0$$

The constants are

$$A_0 = \left(\frac{r_\oplus}{p}\right)^4 e^4 - 2\left(\frac{r_\oplus}{p}\right)^2 \left(r_{\odot y}^2 - r_{\odot x}^2\right) e^2 + \left(r_{\odot x}^2 + r_{\odot y}^2\right)^2$$

$$A_1 = 4\left(\frac{r_\oplus}{p}\right)^4 e^3 - 4\left(\frac{r_\oplus}{p}\right)^2 (r_{\odot y}^2 - r_{\odot x}^2) e$$

$$A_2 = 6\left(\frac{r_\oplus}{p}\right)^4 e^2 - 2\left(\frac{r_\oplus}{p}\right)^2 (r_{\odot y}^2 - r_{\odot x}^2) - 2\left(\frac{r_\oplus}{p}\right)^2 (1 - r_{\odot y}^2) e^2$$

$$+ 2(r_{\odot y}^2 - r_{\odot x}^2)(1 - r_{\odot y}^2) - 4 r_{\odot x}^2 r_{\odot y}^2$$

$$A_3 = 4\left(\frac{r_\oplus}{p}\right)^4 e - 4\left(\frac{r_\oplus}{p}\right)^2 (1 - r_{\odot y}^2) e$$

$$A_4 = \left(\frac{r_\oplus}{p}\right)^4 - 2\left(\frac{r_\oplus}{p}\right)^2 (1 - r_{\odot y}^2) + (1 - r_{\odot y}^2)^2$$

The fourth-order equation may be solved by standard procedures. The two spurious roots may be rejected by noting that $|\hat{r}_\odot \times \vec{r}| = r \sin \psi = |\vec{r}_\oplus|$ and $\hat{r}_\odot \cdot \vec{r}/r \leqq 0$ for occultation to occur.

APPENDIX B

VIEWING POINTS ON THE SUN'S SURFACE FROM A SPACECRAFT

The purpose of this appendix is to develop the equations necessary for locating a point on the Sun's surface as it is viewed from a spacecraft in orbit around the Earth. The symbols used for this appendix form a self-contained set, and they are not all defined in or consistent with the symbol lists in the body of the paper or in appendix A.

a central angle between the intersection of the scanning plane with the solar equator and the sub-Earth meridian, deg (see sketch (B7))

A constant, defined in equation (B7)

B heliographic latitude of the viewing point, deg

B_o heliographic latitude of the sub-Earth point, deg

c central angle between the intersection of the scanning plane with the solar equator and the sub-Earth point, deg (see sketch (B7))

i_ρ angle between the scanning plane and the solar equatorial plane, deg

i_Θ inclination of the solar equator to the ecliptic, deg

J.D. Julian date

ℓ difference in heliographic longitude between the meridian passing through the viewing point and the intersection of the scanning plane with the solar equator, deg (see sketch (B7))

L heliographic longitude of the viewing point, deg

L_o heliographic longitude of the sub-Earth point, deg

M heliographic longitude of the ascending node of the solar equator on the ecliptic, deg

$\hat{P}$ unit vector in the direction of the Sun's north pole, may be specified in an ecliptic coordinate system ($\hat{P}_{ec}$) or in a right-ascension–declination (Earth equatorial) system ($\hat{P}_{eq}$)

$\vec{r}(\hat{r})$ position vector from Earth's center (or unit vector) of a spacecraft, km

$\vec{r}_T$ vector from Earth's center to a point of tangency at the Earth's surface or in its atmosphere, km (see sketch (B1))

$\hat{r}_T(r_{Tx}, r_{Ty}, r_{Tz})$ unit vector in the direction of $\vec{r}_T$

APPENDIX B

S — sub-Earth point on the Sun

$\vec{S}$ — vector from the spacecraft to the point of tangency

SC — spacecraft

V — viewing point on the Sun

$\hat{x}_\Theta(x_\Theta, y_\Theta, z_\Theta)$ — unit vector to the Sun

$\underline{X}$ — matrix defined in equation (B3)

α — angle between $\vec{S}$ and $-\vec{r}$ (see sketch (B1))

ε — obliquity of the Earth's equator to the ecliptic, deg

$\hat{\eta}(\eta_x, \eta_y, \eta_z)$ — unit vector, $\hat{r}_T \times \hat{x}_\Theta$

$\hat{\eta}_\rho$ — unit vector, $\hat{\rho} \times \hat{x}_\Theta$

θ — angular part of a polar coordinate system for describing viewing points on the Sun's surface (see sketch (B2))

Λ — heliocentric longitude of the Earth, deg

ρ — number between 0 and 1 which locates the viewing point relative to the center of the solar disk (see sketch (B6))

$\hat{\rho}(\rho_x, \rho_y, \rho_z)$ — unit vector defining the orientation of the scanning plane relative to the spacecraft

Υ — direction of vernal equinox vector

ψ — central angle, $\sin^{-1} \rho$

Ω_Θ — celestial longitude of the ascending node of the solar equator on the ecliptic, deg

Subscripts:

x,y,z — components of a unit vector along Earth equatorial right-ascension–declination coordinate system

Assume that the Sun is viewed from a spacecraft along a line of sight directed at the center of the solar disk. The "cross hairs" of this viewing system are the projections of $\hat{r}_T$ and $\hat{\eta}$ on the solar disk, where the geometry is as follows:

APPENDIX B

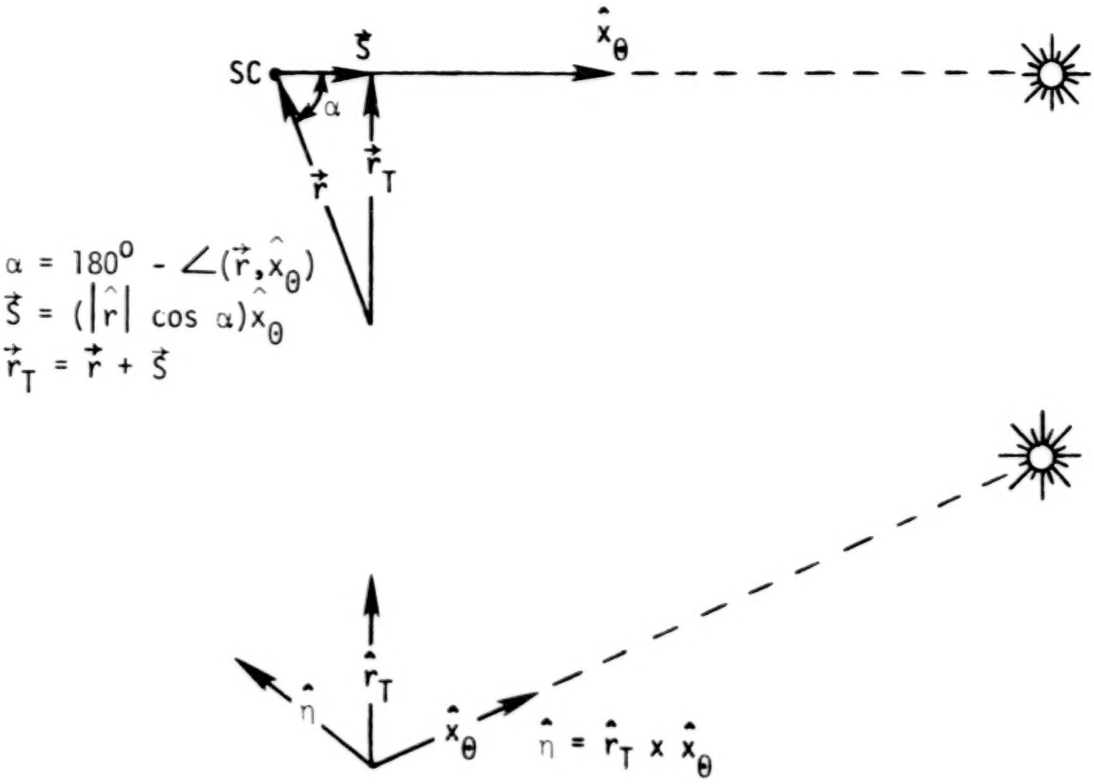

Sketch (B1)

Points on the solar disk are located by the polar coordinate system (ρ,θ) as shown below:

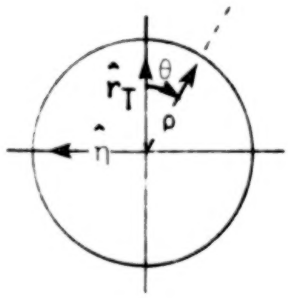

Sketch (B2)

The unit vector $\hat{\rho}$ in the right-ascension–declination system is found by solving the following set of equations, where θ is specified:

$$\left.\begin{aligned} \hat{\rho} \cdot \hat{x}_\theta &= 0 \\ \hat{\rho} \cdot \hat{r}_T &= \cos\theta \\ \hat{\rho} \cdot \hat{\eta} &= -\sin\theta \end{aligned}\right\} \qquad \text{(B1)}$$

Or, in matrix form:

$$\hat{\rho}\underline{X} = [0, \cos\theta, -\sin\theta] \tag{B2}$$

where

$$\underline{X} = \begin{bmatrix} x_\Theta & r_{Tx} & \eta_x \\ y_\Theta & r_{Ty} & \eta_y \\ z_\Theta & r_{Tz} & \eta_z \end{bmatrix} \tag{B3}$$

Then,

$$\hat{\rho} = [0, \cos\theta, -\sin\theta]\underline{X}^{-1} \tag{B4}$$

Algebraically,,

$$\left.\begin{aligned} \rho_x x_\Theta + \rho_y y_\Theta + \rho_z z_\Theta &= 0 \\ \rho_x r_{Tx} + \rho_y r_{Ty} + \rho_z r_{Tz} &= \cos\theta \\ \rho_x \eta_x + \rho_y \eta_y + \rho_z \eta_z &= -\sin\theta \end{aligned}\right\} \tag{B5}$$

and the components of $\hat{\rho}$ are

$$\left.\begin{aligned} \rho_x &= \frac{1}{A}\left[-(r_{Ty}\sin\theta + \eta_y\cos\theta)z_\Theta - (r_{Tz}\sin\theta + \eta_z\cos\theta)y_\Theta\right] \\ \rho_y &= \frac{1}{A}\left[+(r_{Tx}\sin\theta + \eta_x\cos\theta)z_\Theta - (r_{Tz}\sin\theta + \eta_z\cos\theta)x_\Theta\right] \\ \rho_z &= \frac{1}{A}\left[-(r_{Tx}\sin\theta + \eta_x\cos\theta)y_\Theta - (r_{Ty}\sin\theta + \eta_y\cos\theta)x_\Theta\right] \end{aligned}\right\} \tag{B6}$$

where

$$A = (\eta_x r_{Ty} - \eta_y r_{Tx}) z_\Theta + (\eta_z r_{Tx} - \eta_x r_{Tx}) y_\Theta + (\eta_y r_{Tz} - \eta_z r_{Ty}) x_\Theta \tag{B7}$$

The Sun's coordinate system is detailed in reference 7. Specifically, the inclination of the solar equator to the ecliptic and the celestial longitude of the ascending node of the solar equator on the ecliptic are

$$i_\Theta = 7^{\circ}.25 \tag{B8}$$

$$\Omega_\Theta = 73^{\circ}.666667 + 3.821583 \times 10^{-5}(\text{J.D.} - 239\ 6759.5) \tag{B9}$$

where 239 6759.5 is the Julian date (J.D.) for 1850.0 (see ref. 3 for an explanation of time and coordinate systems). A heliographic longitude-latitude system is established on the Sun's surface as follows:

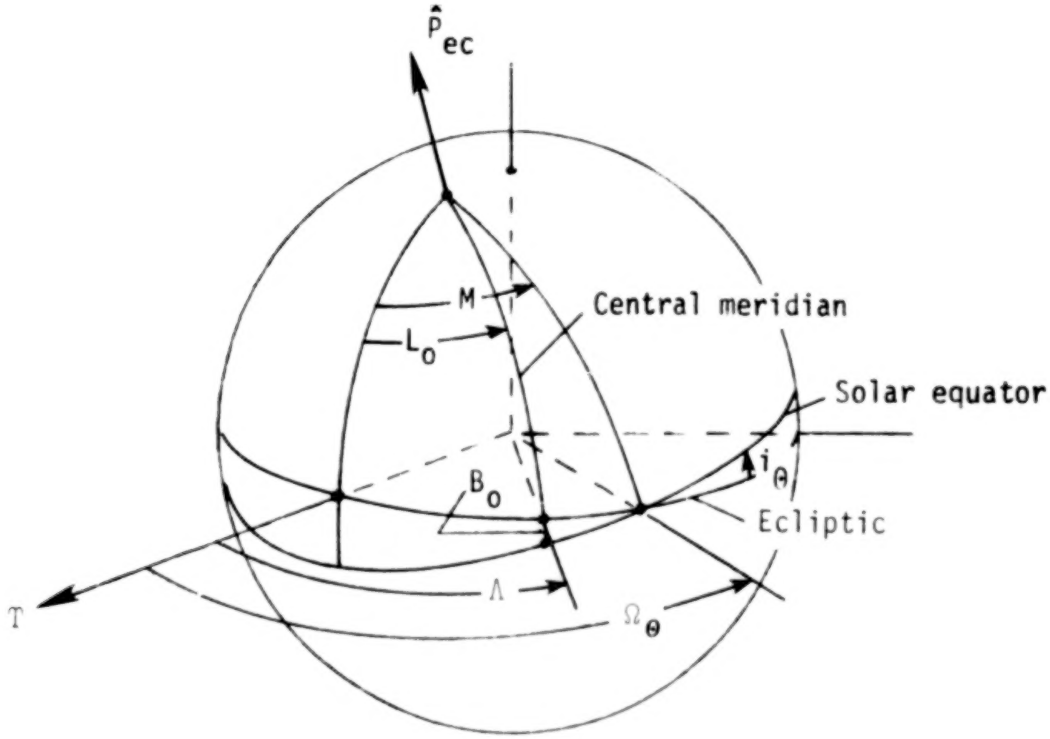

Sketch (B3)

The heliographic longitude of the solar equator ascending node on the ecliptic M is arbitrarily referenced from a solar meridian that passed through the solar equator ascending node at Greenwich mean noon, January 1, 1854, J.D. 239 8220.0. The sidereal rotation period of 25.38 mean solar days is used to establish the Sun's rotation rate of 14.18439716 deg/day, and M is given by

$$M = 292^{\circ}.766 + 14.18439716(243\ 0000.5 - \text{J.D.}) \tag{B10}$$

APPENDIX B

The unit vector for the orientation of the Sun's pole in ecliptic coordinates $\hat{P}_{ec}$ is

$$\left.\begin{aligned} P_{ec,x} &= \sin i_\odot \sin \Omega_\odot \\ P_{ec,y} &= -\sin i_\odot \cos \Omega_\odot \\ P_{ec,z} &= \cos i_\odot \end{aligned}\right\} \qquad \text{(B11)}$$

The central meridian is that meridian which passes through the sub-Earth point S. For all practical purposes S is identical to the subsatellite point for any near-Earth orbit. The sub-Earth coordinates are calculated from the Earth's heliocentric longitude Λ:

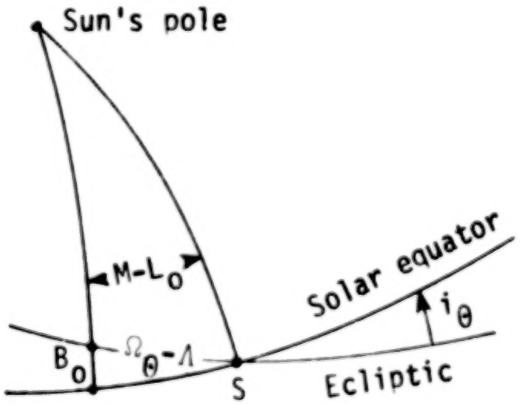

Sketch (B4)

$$\sin(\Omega_\odot - \Lambda) \sin i_\odot = \sin B_o \qquad \text{(B12)}$$

$$\cos(\Omega_\odot - \Lambda) = \cos (90^o - B_o) \cos 90^o + \sin (90^o - B_o) \sin 90^o \cos (M - L_o)$$

$$\cos(\Omega_\odot - \Lambda) = \cos B_o \cos (M - L_o) \qquad \text{(B13)}$$

$$\frac{\sin (90^o - B_o)}{\sin (90^o - i_\odot)} = \frac{\sin (\Omega_\odot - \Lambda)}{\sin (M - L_o)}$$

$$\cos B_o \sin (M - L_o) = \sin (\Omega_\odot - \Lambda) \cos i_\odot \qquad \text{(B14)}$$

Equations (B12), (B13), and (B14) are sufficient to solve unambiguously for the coordinates L_o and B_o.

The projection of $\hat{\rho}$ across the solar disk defines a plane which cuts the Sun in a great circle through the sub-Earth point. The geometry is shown below:

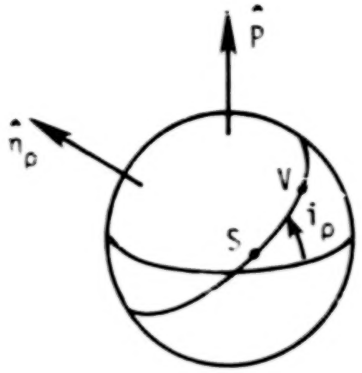

Sketch (B5)

The viewing instrument may scan along the projection of $\hat{\rho}$ to some point V. The angle which the scanning plane makes with the solar equator is required. In an Earth equatorial right-ascension–declination system, this plane is characterized by the unit vector $\hat{\eta}_\rho$:

$$\hat{\eta}_\rho = \hat{\rho} \times \hat{x}_\Theta \tag{B15}$$

Then, the angle between the equator and the scanning plane i_ρ is

$$i_\rho = \cos^{-1} (\hat{\eta}_\rho \cdot \hat{P}_{eq}) \tag{B16}$$

where the unit vector for the Sun's north pole has been transformed from an ecliptic system (see eq. (B11)) into the Earth equatorial right-ascension–declination system:

$$\left.\begin{aligned} P_{eq,x} &= \sin i_\Theta \sin \Omega_\Theta \\ P_{eq,y} &= -\sin i_\Theta \cos \Omega_\Theta \cos \varepsilon - \cos i_\Theta \sin \varepsilon \\ P_{eq,z} &= -\sin i_\Theta \cos \Omega_\Theta \sin \varepsilon + \cos i_\Theta \cos \varepsilon \end{aligned}\right\} \tag{B17}$$

The Earth's obliquity ε is about $23^o.44$.

APPENDIX B

To define the viewing point V along $\hat{\rho}$, consider moving a certain distance away from the center of the solar disk. The geometry is shown below:

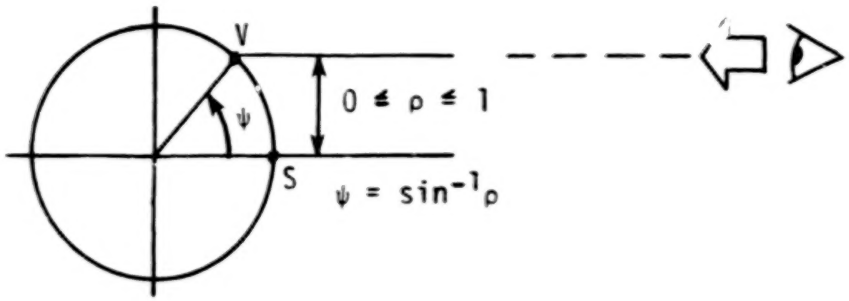

Sketch (B6)

Some fraction of the solar disk, given by ρ between 0 and 1, is converted to a central angle on the surface of the Sun through the relationship for ψ.

The problem is solved now, in principle. Typically, the solution is coded for computer implementation and it is necessary to exercise caution in applying spherical trigonometric relationships. The geometrical relationships are summarized below:

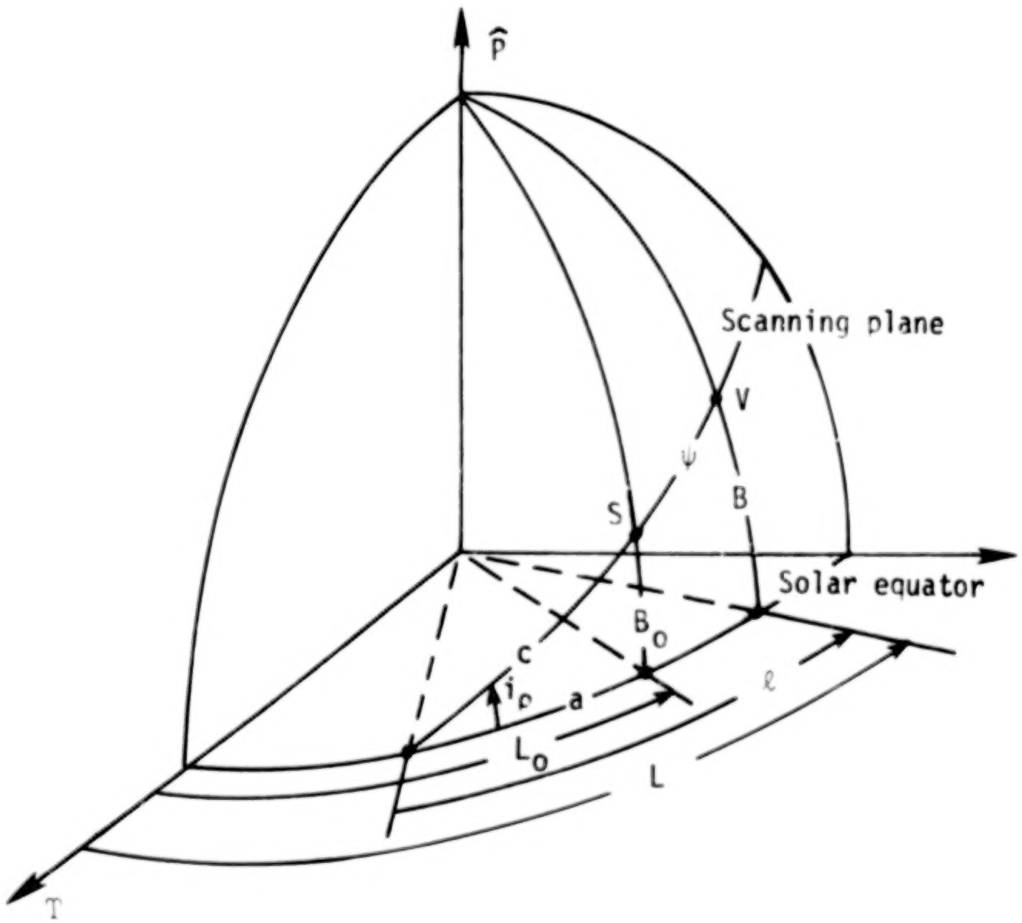

Sketch (7)

Interpretation of these angular quantities is influenced by three factors: the angle between $\hat{\eta}_\rho$ and $\hat{P}$; the angle between $\hat{r}$ and $\hat{P}$ (where $\hat{r}$, $\hat{\eta}_\rho$, and $\hat{P}$ must be expressed in identical coordinate systems, the Earth equatorial right-ascension–declination system, for example); and the value of sub-Earth latitude (specifically, whether B_o is positive or negative). Table B1 summarizes the possibilities. The following trigonometric and logical relationships may be applied:

$$
\left.
\begin{aligned}
i_\rho^* &= \cos^{-1}\left(\hat{\eta}_p \cdot \hat{P}\right) \\
i_\rho &= \begin{cases} i_\rho^* & (i_\rho^* \leq 90^\circ) \\ 180^\circ - i_\rho^* & (i_\rho^* > 90^\circ) \end{cases} \\
c &= \sin^{-1}\left(\sin B_o / \sin i_\rho\right) \\
a &= \sin^{-1}\left(\tan B_o / \tan i_\rho\right) \\
B^* &= \sin^{-1}\left\{\sin i_\rho \sin\left[\psi + \operatorname{sign}\left(\hat{r} \cdot \hat{P}\right) c\right]\right\} \\
L^* &= \sin^{-1}\left(\tan B^* / \tan i_\rho\right) \\
B &= \operatorname{sign}\left(\hat{r} \cdot \hat{P}\right) B^* \\
L &= L_o + \operatorname{sign}\left(\cos i_\rho\right) L^* - \operatorname{sign}\left(\hat{r} \cdot \hat{P}\right) a
\end{aligned}
\right\} \qquad \text{(B18)}
$$

where the sign ( ) function is equal to +1 or -1 depending on the sign of the argument inside the parentheses.

An application of the set of equations (B18) to the nominal 70°, 600-km solar occultation mission described in the main body of the paper (see fig. 4) is illustrated in figure B1. Here, the heliographic latitude for viewing the "top" edge of the Sun's image ($\theta = 0$, $\rho = 1$) and the sub-Earth point are plotted as a function of time from launch for 1 year. As an example of their use, such data, or tabulated versions of them, could perhaps be the basis for a statistical analysis of the effects of sunspot activity on measurement opportunities.

APPENDIX B

TABLE B1.- POSSIBLE GEOMETRIES FOR VIEWING POINTS ON THE SUN

$B_o > 0$	$B_o < 0$	$\hat{\eta}_\rho \cdot \hat{P}$	$\hat{r} \cdot \hat{P}$
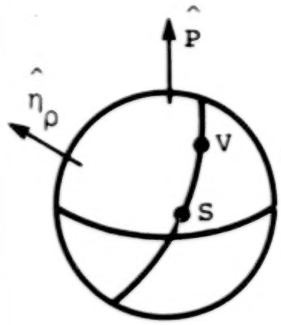	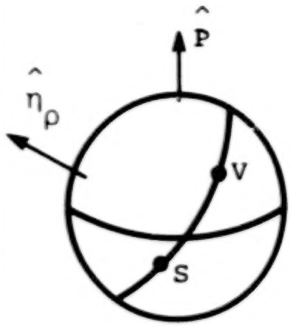	>0	>0
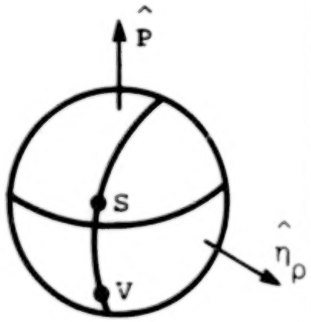	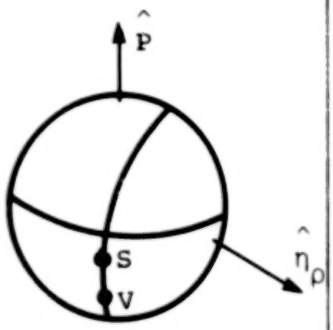	<0	<0
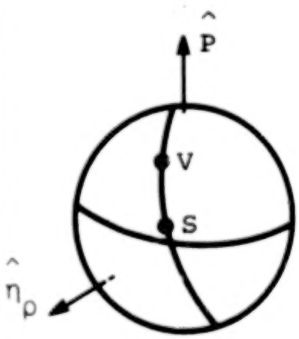	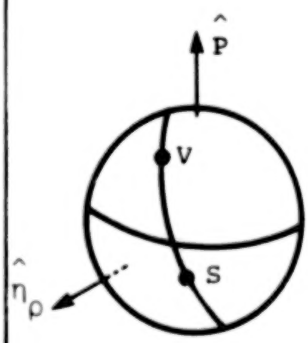	<0	>0
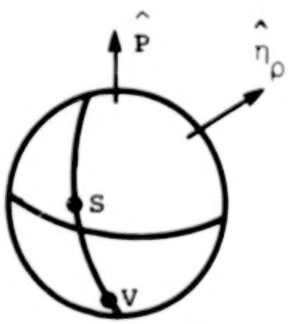	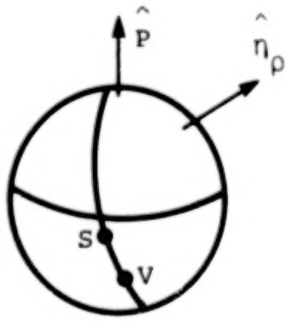	>0	<0

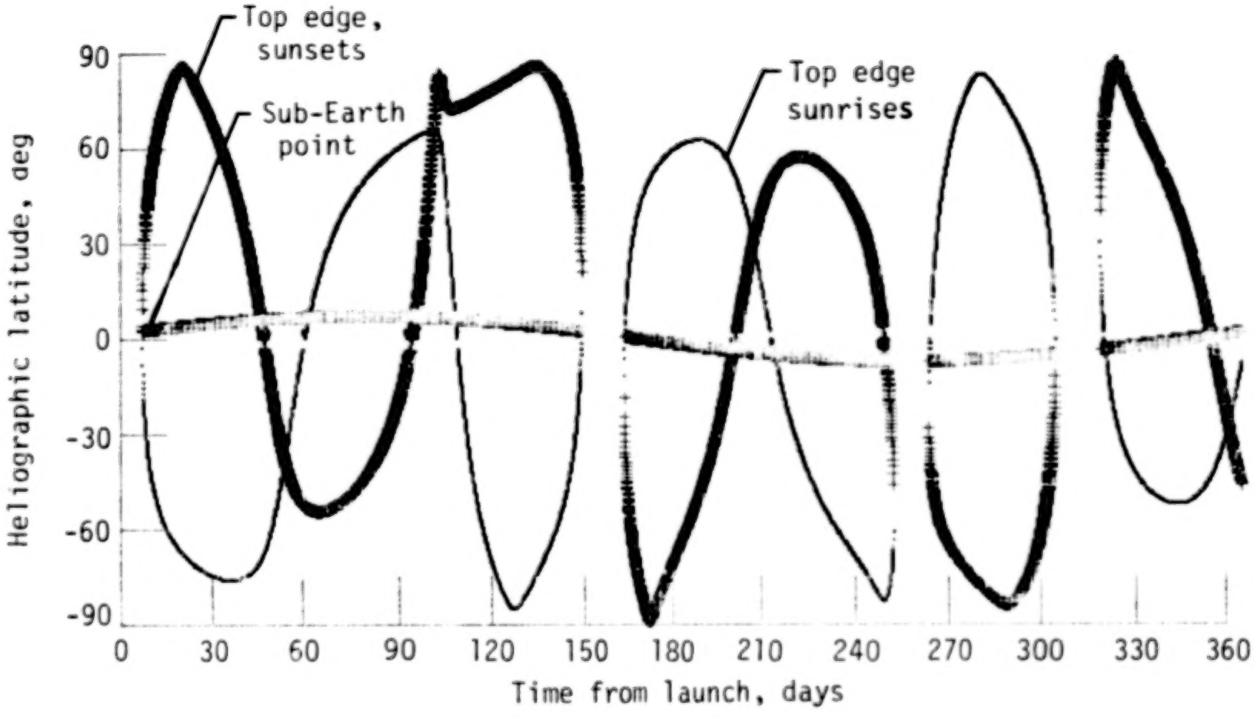

Figure B1.- Heliographic latitude of the subsatellite point and the top edge of the solar disk as viewed during sunrises and sunsets on a 1-year solar occultation mission using a 70°, 600-km circular orbit.

REFERENCES

1. Harrison, Edwin F.; Green, Richard N.; Brooks, David R.; Lawrence, George F.; and McCormick, M. Patrick: Mission Analysis for Satellite Measurements of Stratospheric Constituents by Solar Occultation. Paper presented at the AIAA 13th Aerospace Sciences Meeting (Pasadena, California), Jan. 1975. (Available as AIAA Paper 75-57.)

2. Russell, James M., III; Park, Jae H.; and Drayson, S. Roland: Global Monitoring of Stratospheric Halogen Compounds From a Satellite Using Gas Filter Spectroscopy in the Solar Occultation Mode. Appl. Opt., vol. 16, no. 3, Mar. 1977, pp. 607-612.

3. Brooks, David R.: An Introduction to Orbit Dynamics and Its Application to Satellite-Based Earth Monitoring Missions. NASA RP-1009, 1977.

4. Melbourne, William G.; Mulholland, J. Derral; Sjogren, William L.; and Sturms, Francis M., Jr.: Constants and Related Information for Astrodynamic Calculations, 1968. Tech. Rep. No. 32-1306 (Contract NAS 7-100), Jet Propulsion Lab., California Inst. Technol., July 15, 1968.

5. Allen, C. W.: Astrophysical Quantities. Second ed., Athlone Press, c.1963. (Available from Oxford Univ. Press, Inc., New York.)

6. Escobal, Pedro Ramon: Methods of Orbit Determination. John Wiley & Sons, Inc., c.1965.

7. Explanatory Supplement to the Astronomical Ephemeris and the American Ephemeris and Nautical Almanac. H.M. Naut. Alm. Off., 1961.

TABLE 1.- ORBIT PARAMETERS FOR NOMINAL SOLAR OCCULTATION MISSION

Semimajor axis, a, km	6978
Eccentricity, e	0
Inclination, i, deg	70
Period,[a] sec	5805
Nodal precession rate, $\dot{\Omega}$, deg/day	-2.4868

[a]Nodal period from first-order perturbation theory; 5805-sec period results in 14.883 orbits/day.

TABLE 2.- SLOW PASSAGES OF SUN THROUGH ATMOSPHERE NEAR BEGINNING OF NOMINAL SOLAR OCCULTATION MISSION

Orbit number	Minimum solar altitude, km	Time below 100 km,[a] min
102	52.4	9.1
103	42.0	9.8
104	31.6	10.5
105	21.1	11.2
106	10.5	11.9
107	-.2	12.6
108	-11.0	13.3

[a]The center of the solar disk is at an altitude of less than 100 km above the local horizon.

TABLE 3.- TYPICAL LIMITING CASES FOR VIEWING THE SUN IN THE VICINITY OF THE HORIZON, FROM THE NOMINAL MISSION

	Slow[a]	Fast[b]
Time for measurement while center of Sun is less than 100 km above local horizon, min	12.5	0.81
Change in surface coordinates of tangent point:		
Longitude, deg	18	0.17
Latitude, deg	45	<0.01
Change in pointing angles to center of Sun:		
α, deg	2	2
β, deg	20	<0.01

[a]Center of Sun moves from altitude of 100 km to the horizon and back up to 100 km.

[b]Sunrise or sunset when Sun's vertical motion near the horizon is maximum.

TABLE 4.- DISTRIBUTION OF APPARENT VELOCITY OF SUN'S IMAGE RELATIVE TO HORIZON AS VIEWED FROM A SPACECRAFT DURING NOMINAL SOLAR OCCULTATION MISSION

$\lvert v_{rel} \rvert$, km/sec	Number of events	Cumulative percentage of total events	Measurement time,[a] sec
0-0.1	6	0.06	∞-1000
0.1-0.3	102	1.1	1000-333
0.3-0.5	152	2.7	333-200
0.5-0.7	170	4.5	200-143
0.7-0.9	202	6.7	143-111
0.9-1.1	224	9.0	111-91
1.1-1.3	248	11.6	91-77
1.3-1.5	502	16.9	77-67
1.5-1.7	430	21.5	67-59
1.7-1.9	844	30.4	59-53
1.9-2.1	742	38.2	53-48
2.1-2.3	714	45.7	48-43
2.3-2.5	770	53.9	43-40
2.5-2.7	892	63.3	40-37
2.7-2.9	1156	75.5	37-34
2.9-3.1	2326	100.0	34-32
Total	9480		

[a]Time for the Sun to pass through 100 km of atmosphere at the constant rate v_{rel} (see text).

TABLE 5.- DIVISION OF EARTH INTO ELEMENTS APPROXIMATELY EQUAL IN AREA TO A $5^{o} \times 5^{o}$ BOX AT EQUATOR

Latitude band, deg	Area of band, km^2	ΔL,[a] deg	No.[b]	Area of each box, km^2	Cumulative area, km^2	Percent of hemisphere area	
						In band	Cumulative[c]
0 5	22 277 408	5	72	309 408	22 277 408	8.72	8.7
5 10	22 107 863	5	72	307 053	44 385 271	8.65	17.4
10 15	21 770 064	5	72	302 362	66 155 335	8.52	25.9
15 20	21 266 582	5	72	295 369	87 421 918	8.32	34.2
20 25	20 601 249	5	72	286 128	108 023 167	8.06	42.3
25 30	19 779 127	6	60	329 652	127 802 294	7.74	50.0
30 35	18 806 475	6	60	313 441	146 608 769	7.36	57.4
35 40	17 690 693	6	60	294 844	164 299 462	6.92	64.3
40 45	16 440 275	6	60	274 004	180 739 737	6.43	70.7
45 50	15 064 737	8	45	334 771	195 804 474	5.89	76.6
50 55	13 574 547	8	45	301 656	209 379 021	5.31	81.9
55 60	11 981 046	9	40	299 526	221 360 066	4.69	86.6
60 65	10 296 362	10	36	286 010	231 656 428	4.03	90.6
65 70	8 533 317	12	30	284 443	240 189 745	3.34	94.0
70 75	6 705 328	18	20	335 266	246 895 073	2.62	96.6
75 80	4 826 307	24	15	321 753	251 721 380	1.89	98.5
80 85	2 910 555	40	9	323 395	254 631 935	1.14	99.6
85 90	972 653	120	3	324 217	255 604 588	.38	100.0

[a]Longitude span of each box.
[b]Number of boxes in each latitude band.
[c]From equator to pole.

TABLE 6.- SOLAR POSITION DATA AS A FUNCTION OF TIME

Calendar date, 1981	Days from Jan. 1.0[a]	Days from vernal equinox	$\delta_\odot$, deg	$RA_\odot$, deg
1/ 1	0	-78.7	-23.03	280.56
1/ 6	5	-73.7	-22.53	285.49
1/11	10	-68.7	-21.85	290.42
1/16	15	-63.7	-20.99	295.35
1/21	20	-58.7	-19.97	300.27
1/26	25	-53.7	-18.73	305.20
1/31	30	-48.7	-17.46	310.13
2/ 5	35	-43.7	-16.01	315.06
2/10	40	-38.7	-14.44	319.99
2/15	45	-33.7	-12.73	324.91
2/20	50	-28.7	-11.02	329.84
2/25	55	-23.7	-9.20	334.77
3/ 2	60	-18.7	-7.32	339.70
3/ 7	65	-13.7	-5.39	344.63
3/12	70	-8.7	-3.43	349.56
3/17	75	-3.7	-1.46	354.48
3/22	80	1.3	0.51	359.41
3/27	85	6.3	2.48	4.34
4/ 1	90	11.3	4.43	9.27
4/ 6	95	16.3	6.34	14.20
4/11	100	21.3	8.21	19.13
4/16	105	26.3	10.02	24.05
4/21	110	31.3	11.76	28.98
4/26	115	36.3	13.42	33.91
5/ 1	120	41.3	14.99	38.84
5/ 6	125	46.3	16.45	43.77
5/11	130	51.3	17.80	48.69
5/16	135	56.3	19.03	53.62
5/21	140	61.3	20.12	58.55
5/26	145	66.3	21.07	63.48
5/31	150	71.3	21.87	68.41
6/ 5	155	76.3	22.51	73.34
6/10	160	81.3	22.99	78.26
6/15	165	86.3	23.30	83.19
6/20	170	91.3	23.43	88.12
6/25	175	96.3	23.40	93.05
6/30	180	101.3	23.19	97.98
7/ 5	185	106.3	22.82	102.91
7/10	190	111.3	22.27	107.83
7/15	195	116.3	21.57	112.76
7/20	200	121.3	20.72	117.69
7/25	205	126.3	19.72	122.62
7/30	210	131.3	18.58	127.55
8/ 4	215	136.3	17.32	132.47
8/ 9	220	141.3	15.94	137.40
8/14	225	146.3	14.46	142.33
8/19	230	151.3	12.87	147.26
8/24	235	156.3	11.21	152.19
8/29	240	161.3	9.47	157.12
9/ 3	245	166.3	7.66	162.04
9/ 8	250	171.3	5.81	166.97
9/13	255	176.3	3.91	171.90
9/18	260	181.3	1.99	176.83
9/23	265	186.3	0.04	181.76
9/28	270	191.3	-1.90	186.69
10/ 3	275	196.3	-3.85	191.61
10/ 8	280	201.3	-5.77	196.54
10/13	285	206.3	-7.66	201.47
10/18	290	211.3	-9.51	206.40
10/23	295	216.3	-11.30	211.33
10/28	300	221.3	-13.02	216.25
11/ 2	305	226.3	-14.65	221.18
11/ 7	310	231.3	-16.19	226.11
11/12	315	236.3	-17.61	231.04
11/17	320	241.3	-18.91	235.97
11/22	325	246.3	-20.07	240.90
11/27	330	251.3	-21.07	245.82
12/ 2	335	256.3	-21.91	250.75
12/ 7	340	261.3	-22.58	255.68
12/12	345	266.3	-23.06	260.61
12/17	350	271.3	-23.35	265.54
12/22	355	276.3	-23.44	270.47
12/27	360	281.3	-23.34	275.39
1/ 1	365	286.3	-23.05	280.32

[a]0h GMT.

TABLE 7.- MAXIMUM TANGENT LATITUDE AVAILABLE DURING SOLAR OCCULTATION MISSION AS A FUNCTION OF ORBIT INCLINATION AND ALTITUDE

Altitude, km	Maximum northern or southern tangent latitude, deg, for specified orbit inclination, deg, of -										[a] i_{polar}, deg
	0	10	20	30	40	50	60	70	80	90	
200	14.2	24.2	34.2	44.2	54.2	64.2	74.2	84.2	90	90	75.8
400	19.8	29.8	39.8	49.8	59.8	69.8	79.8	89.9	90	90	70.2
600	23.9	33.9	43.9	53.9	63.9	73.9	83.9	90	90	90	66.1
800	27.3	37.3	47.3	57.3	67.3	77.3	87.3	90	90	90	62.7
1000	30.2	40.2	50.2	60.2	70.2	80.2	90	90	90	90	59.8
1200	32.7	42.7	52.7	62.7	72.7	82.7	90	90	90	90	57.3
1400	34.9	44.9	54.9	64.9	74.9	84.9	90	90	90	90	55.1
1600	36.9	46.9	56.9	66.9	76.9	86.9	90	90	90	90	53.1

[a]Minimum inclination for polar coverage at the specified altitude.

TABLE 8.- NODAL PRECESSION RATES FOR CIRCULAR ORBITS AS A FUNCTION OF ALTITUDE AND INCLINATION

i, deg	$\dot{\Omega}$, deg/day, at altitude, h, km, of -													
	200	300	400	500	600	700	800	900	1000	1100	1200	1300	1400	1500
0	-8.956	-8.495	-8.064	-7.661	-7.283	-6.929	-6.597	-6.285	-5.992	-5.716	-5.456	-5.211	-4.980	-4.762
10	-8.820	-8.366	-7.941	-7.544	-7.172	-6.824	-6.496	-6.189	-5.900	-5.629	-5.373	-5.132	-4.904	-4.690
20	-8.414	-7.981	-7.576	-7.197	-6.842	-6.510	-6.198	-5.905	-5.629	-5.370	-5.126	-4.896	-4.679	-4.474
30	-7.752	-7.353	-6.980	-6.631	-6.304	-5.998	-5.710	-5.440	-5.187	-4.948	-4.723	-4.511	-4.311	-4.123
40	-6.855	-6.502	-6.172	-5.864	-5.575	-5.304	-5.050	-4.811	-4.586	-4.375	-4.176	-3.989	-3.812	-3.646
50	-5.749	-5.454	-5.177	-4.918	-4.676	-4.449	-4.236	-4.035	-3.847	-3.670	-3.503	-3.346	-3.198	-3.058
60	-4.471	-4.241	-4.026	-3.825	-3.636	-3.460	-3.294	-3.138	-2.992	-2.854	-2.724	-2.602	-2.487	-2.378
70	-3.057	-2.900	-2.753	-2.615	-2.487	-2.366	-2.252	-2.146	-2.046	-1.952	-1.863	-1.780	-1.701	-1.626
80	-1.552	-1.472	-1.397	-1.328	-1.262	-1.201	-1.143	-1.089	-1.039	-.991	-.946	-.903	-.863	-.826
90	0	0	0	0	0	0	0	0	0	0	0	0	0	0
100	1.552	1.472	1.397	1.328	1.262	1.201	1.143	1.089	1.039	.991	.946	.903	.863	.826

TABLE 9.- AVERAGE AND STANDARD DEVIATION OF q AS A FUNCTION OF LATITUDE BAND AND TIME FOR NOMINAL SOLAR OCCULTATION MISSION

Latitude band, deg	n_q	$\bar{q}$	s_q	$\bar{t}$, days	t_{first}, days	t_{last}, days
-90 -85	68	25.661	4.136	76.748	74.498	78.999
-85 -80	21	26.182	3.343	73.759	73.087	74.430
	51	27.936	5.135	80.746	79.066	82.426
-80 -75	135	25.967	4.250	48.419	43.917	52.921
	15	27.772	6.288	72.550	72.080	73.020
	59	30.976	5.559	84.441	82.493	86.390
-75 -70	194	34.624	5.541	241.426	234.940	247.911
	139	31.524	5.422	308.910	304.274	313.546
	52	28.515	5.563	42.136	40.422	43.850
	33	28.656	4.086	54.063	52.988	55.138
	10	29.391	3.976	71.711	71.409	72.013
	61	30.486	4.492	88.473	86.457	90.489
-70 -65	62	34.689	4.439	232.823	230.772	234.873
	74	34.618	6.072	250.432	247.978	252.885
	49	36.057	5.156	302.594	300.981	304.207
	29	34.241	5.718	314.554	313.613	315.494
	97	34.029	5.517	348.097	344.872	351.323
	41	29.833	5.235	39.011	37.667	40.355
	20	29.744	4.644	55.843	55.205	56.481
	7	26.608	4.740	71.140	70.939	71.342
	58	30.303	5.520	92.472	90.556	94.387
-65 -60	218	35.534	5.496	205.142	197.851	212.434
	33	35.927	6.783	229.630	228.554	230.705
	47	36.027	5.837	254.498	252.952	256.044
	39	37.387	6.080	299.637	298.361	300.914
	20	35.382	4.862	316.199	315.561	316.837
	41	34.065	5.096	343.462	342.118	344.805
	56	34.845	5.166	353.238	351.390	355.086
	36	31.893	4.433	36.423	35.247	37.600
	13	29.397	4.648	56.951	56.548	57.354
	5	30.459	4.002	70.738	70.604	70.872
	50	30.808	5.477	96.101	94.454	97.747
	60	32.595	6.032	145.010	143.028	146.993
-60 -55	137	35.189	5.992	193.214	188.643	197.784
	79	36.715	5.871	215.123	212.501	217.744
	23	37.276	7.024	227.747	227.007	228.487
	35	37.409	5.049	257.254	256.111	258.397
	35	39.774	6.108	297.151	296.008	298.293
	15	38.535	4.894	317.374	316.904	317.844
	24	37.441	5.103	341.278	340.506	342.051
	40	37.003	6.257	356.464	355.153	357.774
	32	33.717	5.181	34.138	33.096	35.180
	9	33.551	5.860	57.689	57.421	57.958
	3	32.648	6.401	70.470	70.403	70.537

TABLE 9.- Continued

Latitude band, deg	n_q	$\bar{q}$	s_q	$\bar{t}$, days	t_{first}, days	t_{last}, days
-60 -55	41	31.294	4.090	99.159	97.814	100.503
	123	31.780	5.306	138.861	134.760	142.960
	153	32.258	5.034	152.168	147.060	157.276
-55 -50	54	34.305	6.175	186.795	185.014	188.576
	35	38.288	7.586	218.954	217.811	220.097
	18	36.945	5.808	226.368	225.797	226.940
	27	40.473	6.362	259.338	258.464	260.212
	29	40.560	6.804	295.000	294.059	295.941
	12	37.695	5.417	318.281	317.912	318.650
	18	35.772	6.033	339.868	339.297	340.439
	33	34.741	5.956	358.917	357.841	359.992
	28	31.785	4.825	32.122	31.214	33.029
	6	26.395	5.393	58.193	58.025	58.360
	1	27.824		70.337		
	32	30.665	5.205	101.612	100.570	102.654
	42	32.855	5.174	133.315	131.937	134.693
	58	33.825	5.797	159.259	157.343	161.174
-50 -45	30	35.435	5.076	183.972	182.997	184.946
	24	34.538	6.863	220.938	220.164	221.711
	15	36.578	5.861	225.259	224.788	225.730
	24	39.186	6.689	261.052	260.279	261.825
	26	38.398	6.157	293.152	292.311	293.992
	10	36.522	7.774	319.019	318.717	319.321
	13	37.143	5.118	338.827	338.425	339.230
	29	32.028	4.232	361.000	360.059	361.941
	25	30.718	6.295	30.340	29.534	31.147
	4	32.588	7.994	58.528	58.427	58.628
	26	31.345	4.127	103.561	102.721	104.402
	25	32.399	5.110	131.063	130.256	131.870
	37	33.629	5.435	162.452	161.242	163.662
-45 -40	19	33.777	5.801	182.324	181.719	182.929
	33	37.060	7.693	223.189	221.778	224.721
	19	37.732	6.154	262.498	261.892	263.103
	23	35.349	5.176	291.505	290.765	292.244
	7	39.824	5.275	319.589	319.388	319.791
	10	35.170	7.414	338.055	337.753	338.357
	25	32.293	4.718	362.815	362.008	363.622
	23	28.791	4.686	28.727	27.988	29.466
	2	28.147	4.969	58.729	58.695	58.762
	20	28.538	4.848	105.108	104.469	105.746
	18	31.119	5.477	129.617	129.045	130.189
	28	33.665	5.775	164.637	163.729	165.544
-40 -35	13	33.440	5.377	181.248	180.844	181.652
	28	34.141	5.619	223.456	222.972	223.997
	17	34.652	6.932	263.708	263.170	264.246
	20	34.019	8.102	290.059	289.421	290.698
	6	31.961	3.440	320.025	319.858	320.193
	9	34.182	6.926	337.418	337.149	337.686
	23	32.007	5.754	364.428	363.689	365.168

TABLE 9.- Continued

Latitude band, deg	n_q	$\bar{q}$	s_q	$\bar{t}$, days	t_{first}, days	t_{last}, days
-40 -35	22	27.580	5.169	27.251	26.576	27.920
	1	35.398		58.829		
	1	26.947		70.339		
	17	29.780	3.394	106.352	105.814	106.890
	14	28.454	4.424	128.541	128.104	128.978
	23	32.181	6.826	166.351	165.612	167.091
	3	31.804	3.151	172.047	171.980	172.114
-35 -30	9	32.202	4.300	180.508	180.239	180.777
	12	34.426	4.799	222.534	222.164	222.904
	14	34.016	5.310	224.502	224.065	224.939
	15	32.964	4.149	264.784	264.313	265.255
	18	36.362	5.651	288.782	288.210	289.353
	5	35.918	4.129	320.394	320.260	320.528
	6	32.121	3.562	336.915	336.747	337.082
	1	37.371		365.235		
	20	29.274	4.628	.699	.060	1.338
	19	28.322	4.651	25.903	25.298	26.508
	2	27.517	1.744	70.441	70.407	70.474
	13	29.994	5.335	107.360	106.957	107.764
	11	28.232	5.123	127.700	127.364	128.036
	19	33.269	3.686	167.763	167.158	168.368
	20	32.098	4.634	171.274	170.635	171.912
-30 -25	6	34.832	2.187	180.003	179.834	180.171
	11	32.029	3.276	221.761	221.424	222.097
	12	31.418	6.845	225.376	225.006	225.746
	13	33.317	7.696	265.726	265.322	266.129
	16	31.295	5.657	287.639	287.134	288.143
	4	28.423	6.175	320.696	320.595	320.796
	6	31.567	5.071	336.512	336.345	336.680
	20	27.217	5.199	2.043	1.405	2.682
	18	28.230	4.440	24.659	24.088	25.231
	3	26.433	3.256	70.610	70.542	70.677
	11	28.153	4.139	108.168	107.831	108.504
	8	27.936	4.820	127.061	126.825	127.296
	36	28.626	4.456	169.502	168.436	170.568
-25 -20	5	23.828	5.124	179.632	179.497	179.767
	11	30.699	5.800	221.021	220.684	221.357
	12	30.780	4.094	226.184	225.814	226.554
	12	28.771	5.251	266.566	266.196	266.936
	14	28.483	6.080	286.630	286.193	287.067
	3	23.995	2.718	320.930	320.863	320.997
	4	27.004	3.090	336.177	336.077	336.278
	18	28.045	5.107	3.321	2.749	3.892
	16	26.577	4.452	23.516	23.012	24.021
	2	21.475	6.447	58.792	58.758	58.826
	3	29.946	6.662	70.812	70.745	70.879
	9	25.830	3.139	108.841	108.571	109.110
	7	30.739	5.992	126.556	126.354	126.758
	34	27.347	5.163	169.502	168.281	170.722

TABLE 9.- Continued

Latitude band, deg	n_q	$\bar{q}$	s_q	$\bar{t}$, days	t_{first}, days	t_{last}, days
-20 -15	3	30.171	7.279	179.362	179.295	179.430
	12	29.709	4.112	220.247	219.877	220.617
	12	28.683	5.066	226.991	226.621	227.361
	10	25.135	5.150	267.306	267.004	267.609
	13	28.814	4.036	285.722	285.319	286.126
	2	28.184	4.191	321.097	321.064	321.130
	3	26.343	1.803	335.943	335.876	336.010
	16	25.990	5.715	4.464	3.960	4.968
	16	27.156	3.135	22.440	21.936	22.945
	2	25.586	1.908	58.657	58.623	58.691
	4	22.377	1.552	71.048	70.947	71.149
	7	29.820	3.470	109.379	109.177	109.581
	5	24.404	4.228	126.152	126.017	126.286
	15	25.969	3.452	167.743	167.272	168.214
	15	25.518	4.760	171.260	170.789	171.731
-15 -10	2	27.529	.605	179.193	179.160	179.227
	11	25.982	3.103	219.474	219.137	219.810
	12	26.756	3.269	227.798	227.428	228.168
	10	27.814	4.709	267.979	267.676	268.282
	12	26.847	4.038	284.881	284.511	285.251
	1	24.742		321.197		
	2	29.093	5.309	335.776	335.743	335.809
	16	27.115	5.084	5.540	5.036	6.044
	15	26.358	3.818	21.398	20.927	21.869
	3	29.312	5.804	58.488	58.421	58.556
	5	27.961	6.130	71.351	71.217	71.486
	6	23.146	3.439	109.817	109.648	109.985
	4	28.917	3.383	125.848	125.747	125.950
	16	25.723	4.911	166.701	166.196	167.205
	6	24.913	4.769	171.966	171.798	172.135
-10 -5	1	22.273		179.091		
	12	23.663	4.573	218.700	218.330	219.070
	11	27.061	3.762	228.572	228.235	228.908
	9	24.942	3.834	268.618	268.349	268.888
	10	27.014	3.832	284.141	283.839	284.444
	1	26.511		335.676		
	15	27.537	4.416	6.582	6.112	7.053
	15	25.347	5.182	20.389	19.918	20.860
	4	24.710	3.177	58.252	58.151	58.353
	5	23.646	2.141	71.688	71.554	71.823
	5	26.978	5.837	110.187	110.052	110.322
	3	26.172	3.415	125.612	125.545	125.680
	15	25.316	4.545	165.658	165.187	166.129
-5 0	13	25.336	5.624	217.859	217.456	218.263
	12	25.554	3.496	229.345	228.975	229.715
	8	23.986	3.517	269.190	268.955	269.426
	10	27.544	4.764	283.469	283.166	283.771
	1	20.448		335.610		
	15	23.081	5.744	7.591	7.120	8.062

TABLE 9.- Continued

Latitude band, deg	n_q	$\bar{q}$	s_q	$\bar{t}$, days	t_{first}, days	t_{last}, days
-5 0	14	27.084	4.405	19.414	18.977	19.851
	4	21.767	1.731	57.982	57.881	58.083
	6	28.419	5.608	72.059	71.890	72.227
	3	26.468	6.365	110.457	110.389	110.524
	3	26.293	4.866	125.410	125.342	125.477
	15	24.643	3.870	164.649	164.179	165.120
0 5	1	26.336		179.090		
	12	24.839	3.287	217.018	216.648	217.388
	12	26.808	3.886	230.153	229.783	230.523
	8	24.739	4.013	269.729	269.493	269.964
	9	23.967	4.128	282.829	282.560	283.099
	2	27.405	1.628	321.161	321.127	321.195
	1	26.141		335.611		
	14	24.431	3.833	8.566	8.129	9.003
	14	24.846	4.983	18.472	18.035	18.910
	6	27.674	3.672	57.645	57.477	57.814
	6	26.466	3.223	72.463	72.294	72.631
	3	21.474	4.288	110.659	110.592	110.727
	1	19.184		125.274		
	15	24.406	3.710	163.641	163.170	164.111
5 10	2	27.434	4.512	179.190	179.157	179.223
	14	25.681	4.074	216.144	215.707	216.581
	12	24.297	3.433	230.960	230.590	231.330
	7	24.568	2.052	270.234	270.032	270.436
	8	22.843	4.870	282.257	282.022	282.493
	2	24.288	1.308	321.025	320.991	321.059
	1	28.050		335.679		
	14	24.740	4.288	9.508	9.071	9.945
	14	23.695	5.057	17.531	17.094	17.968
	5	25.435	6.132	57.275	57.140	57.410
	8	26.427	5.558	72.934	72.698	73.169
	3	25.123	.828	110.862	110.794	110.929
	1	21.106		125.207		
	16	25.087	3.515	162.598	162.094	163.103
10 15	3	24.352	6.974	179.357	179.290	179.424
	14	26.452	4.640	215.203	214.765	215.640
	13	25.[illegible]88	2.317	231.801	231.397	232.204
	7	25.[illegible]15	4.441	270.705	270.503	270.907
	8	25.517	3.626	281.719	281.483	281.955
	4	25.850	2.969	320.823	320.722	320.924
	2	27.960	5.629	335.781	335.747	335.814
	13	24.719	2.558	10.416	10.012	10.819
	14	25.164	4.758	16.589	16.152	17.026
	8	31.358	4.235	56.862	56.669	57.073
	9	25.104	3.356	73.506	73.237	73.775
	1	24.555		110.997		
	16	27.646	5.554	161.522	161.018	162.027
15 20	3	25.262	3.407	179.558	179.491	179.625
	16	26.973	4.080	214.194	213.689	214.698

TABLE 9.- Continued

Latitude band, deg	n_q	$\bar{q}$	s_q	$\bar{t}$, days	t_{first}, days	t_{last}, days
15 20	14	28.884	3.100	232.709	232.271	233.146
	7	25.955	5.434	271.176	270.974	271.378
	7	23.981	2.322	281.214	281.012	281.416
	4	24.528	3.140	320.553	320.452	320.654
	4	25.460	2.009	335.983	335.882	336.084
	14	27.616	4.544	11.324	10.887	11.761
	14	26.950	3.076	15.648	15.210	16.085
	8	28.301	3.886	56.366	56.130	56.602
	10	30.435	4.675	74.145	73.842	74.448
	1	32.529		111.065		
	1	31.165		125.205		
	17	28.910	4.013	160.413	159.875	160.951
20 25	4	27.365	1.420	179.826	179.692	179.960
	17	26.412	4.238	213.084	212.546	213.622
	15	27.431	4.823	233.684	233.213	234.155
	6	24.541	3.514	271.614	271.446	271.782
	7	26.027	3.955	280.743	280.541	280.945
	6	27.957	4.098	320.216	320.048	320.385
	5	21.097	1.283	336.287	336.152	336.421
	15	28.919	4.647	12.299	11.828	12.770
	16	27.692	4.389	14.639	14.134	15.143
	9	28.550	6.598	55.794	55.525	56.063
	12	30.849	4.346	74.885	74.515	75.255
	2	27.251	.643	125.305	125.271	125.338
	18	29.245	4.640	159.236	158.665	159.808
25 30	6	30.381	2.764	180.194	180.027	180.362
	18	26.703	4.683	211.908	211.336	212.479
	16	30.008	2.620	234.726	234.222	235.231
	7	26.579	1.696	272.032	271.850	272.186
	7	24.528	4.988	280.272	280.070	280.474
	9	26.907	4.410	319.711	319.442	319.980
	6	27.893	4.405	336.657	336.489	336.825
	32	28.827	4.363	13.425	12.837	14.067
	10	30.484	3.443	55.155	54.852	55.457
	13	29.347	5.271	75.726	75.322	76.129
	1	34.970		111.066		
	3	30.896	4.206	125.472	125.405	125.539
	20	29.499	4.701	157.959	157.320	158.597
30 35	7	33.529	3.545	180.630	180.429	180.831
	21	28.274	4.572	210.597	209.924	211.269
	18	26.439	5.326	235.869	235.298	236.441
	5	26.381	1.784	272.389	272.254	272.523
	6	28.961	6.926	279.834	279.666	280.002
	10	26.401	5.278	319.072	318.769	319.375
	9	28.296	5.077	337.162	336.893	337.431
	35	29.480	5.069	13.339	11.781	14.922
	13	31.005	6.306	54.381	53.977	54.785
	16	33.124	5.142	76.701	76.197	77.205
	2	38.229	2.012	110.967	110.933	111.000

TABLE 9.- Continued

Latitude band, deg		n_q	$\bar{q}$	s_q	$\bar{t}$, days	t_{first}, days	t_{last}, days
30	35	5	30.783	4.531	125.740	125.606	125.874
		21	31.931	5.971	156.580	155.908	157.253
35	40	8	30.199	4.152	181.133	180.898	181.368
		22	30.484	5.241	209.151	208.445	209.857
		19	27.340	4.389	237.113	236.508	237.718
		6	30.168	5.303	272.759	272.591	272.927
		6	30.535	2.442	279.430	279.262	279.598
		15	27.836	5.840	318.231	317.760	318.702
		12	27.022	5.108	337.869	337.498	338.239
		22	31.420	5.511	11.007	10.301	11.713
		18	31.286	5.473	15.561	14.989	16.132
		15	32.777	4.649	53.439	52.969	53.910
		18	36.612	5.379	77.844	77.273	78.416
		3	32.479	1.109	110.800	110.733	110.867
		5	32.031	6.972	126.075	125.941	126.209
		22	32.807	4.917	155.135	154.429	155.841
40	45	11	32.341	5.991	181.771	181.435	182.106
		25	31.518	5.015	207.572	206.765	208.378
		21	27.280	5.830	238.458	237.786	239.130
		5	25.687	5.318	273.129	272.995	273.264
		6	27.315	7.262	279.026	278.858	279.194
		19	27.810	3.835	317.088	316.483	317.693
		18	29.438	4.143	338.878	338.306	339.449
		28	35.174	5.831	9.326	8.419	10.234
		21	33.237	6.271	16.872	16.200	17.545
		18	36.353	5.461	52.330	51.758	52.901
		21	36.644	5.817	79.155	78.483	79.827
		4	32.576	6.438	110.565	110.465	110.666
		8	35.013	3.800	126.511	126.276	126.745
		26	32.968	5.566	153.522	152.681	154.362
45	50	13	34.420	5.722	182.576	182.173	182.979
		29	32.292	4.413	205.757	204.816	206.698
		24	28.522	5.728	239.971	239.197	240.744
		6	26.848	2.706	273.500	273.332	273.668
		5	27.186	3.082	278.655	278.521	278.790
		27	29.294	4.930	315.541	314.667	316.415
		28	28.766	5.357	340.424	339.516	341.332
		39	33.522	4.396	7.074	5.797	8.352
		26	33.004	7.134	18.452	17.612	19.293
		24	37.124	5.732	50.918	50.144	51.691
		25	38.394	6.348	80.701	79.895	81.508
		6	38.470	5.673	110.230	110.063	110.398
		10	39.183	9.846	127.115	126.813	127.417
		27	37.383	6.616	151.740	150.866	152.614
50	55	17	34.507	6.490	183.583	183.046	184.121
		32	34.118	4.932	203.707	202.665	204.748
		27	30.671	5.148	241.685	240.811	242.559
		5	30.377	5.857	273.870	273.736	274.005
		6	32.754	6.227	278.285	276.117	278.453

TABLE 9.- Continued

Latitude band, deg	n_q	$\bar{q}$	s_q	$\bar{t}$, days	t_{first}, days	t_{last}, days
50 55	40	29.064	5.337	313.289	311.979	314.600
	55	32.630	5.581	343.214	341.399	345.029
	68	34.518	5.087	3.478	1.226	5.730
	35	35.413	5.828	20.503	19.360	21.646
	31	40.290	7.053	49.069	48.060	50.077
	30	38.366	5.370	82.550	81.575	83.524
	7	41.417	6.598	109.794	109.593	109.996
	13	38.759	5.616	127.887	127.484	128.289
	32	35.471	6.218	149.757	148.716	150.799
55 60	22	34.393	4.199	184.893	184.188	185.598
	40	34.246	6.051	201.302	200.044	202.598
	31	32.032	5.789	243.634	242.626	244.642
	6	30.978	1.494	274.241	274.073	274.409
	5	26.081	3.566	277.915	277.780	278.049
	59	30.535	5.703	309.962	308.013	311.911
	300	33.357	5.643	355.144	345.096	365.191
	18	34.886	6.805	.588	.016	1.159
	55	39.732	6.378	23.528	21.713	25.343
	49	40.755	6.403	46.380	44.767	47.993
	34	41.275	8.025	84.701	83.592	85.810
	9	42.032	6.570	109.258	108.989	109.526
	18	37.177	6.765	128.927	128.357	129.498
	36	38.468	6.571	147.472	146.296	148.648
60 65	35	37.354	5.640	186.807	185.665	187.949
	51	33.732	6.151	198.297	196.617	199.977
	35	30.899	4.546	245.852	244.710	246.995
	5	32.995	4.785	274.611	274.477	274.746
	5	33.019	2.253	277.578	277.443	277.712
	88	29.616	4.651	305.023	302.099	307.946
	288	39.655	6.887	35.055	25.410	44.699
	39	40.385	8.014	87.154	85.877	88.431
	12	43.536	7.694	108.553	108.184	108.922
	27	40.856	6.654	130.438	129.565	131.312
	44	39.316	7.237	144.784	143.339	146.229
65 70	128	37.071	6.395	192.283	188.016	196.549
	42	30.776	5.562	248.440	247.062	249.818
	7	29.283	1.888	275.015	274.813	275.217
	6	28.247	4.050	277.207	277.039	277.376
	113	28.685	4.556	298.269	294.506	302.032
	44	43.460	7.941	89.943	88.498	91.387
	16	40.793	5.012	107.613	107.109	108.116
	55	41.352	6.510	133.193	131.379	135.007
	71	41.087	7.592	140.920	138.568	143.272
70 75	48	32.906	6.217	251.411	249.885	252.976
	16	29.082	4.904	276.043	275.285	276.971
	127	27.617	4.136	290.205	285.971	294.438
	49	42.899	7.144	93.067	91.455	94.680
	22	43.501	7.304	106.337	105.632	107.042
	52	43.508	7.943	136.787	135.074	138.501

TABLE 9.- Concluded

Latitude band, deg	n_q	$\bar{q}$	s_q	$\bar{t}$, days	t_{first}, days	t_{last}, days
75 80	56	33.257	5.522	254.892	253.044	256.740
	155	26.908	4.465	280.756	275.958	285.904
	59	45.621	8.094	96.696	94.747	98.645
	36	45.854	6.804	104.389	103.213	105.564
80 85	67	33.024	5.819	259.025	256.807	261.242
	9	28.304	5.352	275.894	275.625	276.163
	67	47.808	7.041	100.929	98.712	103.146
85 90	213	28.542	5.081	268.433	261.310	275.557

TABLE 10.- LEAST SQUARES PARAMETERS AND RELATED QUANTITIES FOR MODELING BEHAVIOR OF $\bar{q}$ WITHIN A LATITUDE BAND

Latitude band, deg		$n_{\bar{q}}$	Model parameters			s_R^2	R, %
			Q [a]	A [a]	γ, deg		
-90	-85	1					
-85	-80	2					
-80	-75	3	63.84	38.03	-142.9		100.0
-75	-70	6	31.86	3.41	-115.9	0.05	99.4
-70	-65	9	32.07	3.54	175.8	1.70	87.4
-65	-60	12	33.67	3.24	-172.8	.61	92.5
-60	-55	14	35.30	3.75	163.1	.28	96.8
-55	-50	13	34.35	5.60	-172.4	2.46	89.7
-50	-45	13	34.38	3.49	-172.6	2.03	78.0
-45	-40	12	33.34	5.02	-168.5	2.72	84.6
-40	-35	14	32.02	2.50	-168.9	5.19	40.9
-35	-30	15	32.09	3.45	-175.7	5.11	54.2
-30	-25	13	29.73	2.88	-146.8	3.03	62.2
-25	-20	14	27.40	1.40	-127.6	8.37	13.3
-20	-15	15	26.89	1.45	-149.0	4.66	21.3
-15	-10	15	26.85	.62	32.1	3.27	7.1
-10	-5	13	25.53	.88	115.6	2.60	15.3
-5	0	12	25.06	1.25	-59.6	6.06	13.0
0	5	14	24.90	1.35	138.2	5.16	18.3
5	10	14	24.91	.08	85.4	3.69	.1
10	15	13	25.98	.69	12.4	4.63	6.3
15	20	14	27.65	2.85	-18.9	2.54	67.2
20	25	13	27.34	2.11	-11.8	4.29	38.3
25	30	13	28.99	2.69	-16.8	3.03	62.8
30	35	13	30.20	3.66	-17.0	4.56	67.6
35	40	14	30.92	2.66	-4.5	2.96	60.4
40	45	14	31.64	4.52	6.5	2.38	84.6
45	50	14	33.16	5.95	-11.8	.49	97.9
50	55	14	34.93	4.68	-1.2	2.42	85.4
55	60	14	35.32	5.99	2.4	3.09	88.2
60	65	11	36.52	5.29	-2.2	2.74	89.7
65	70	9	35.49	6.76	-17.6	.96	98.2
70	75	6	35.83	8.45	-41.0	.66	99.3
75	80	4	36.19	14.90	-59.0	.89	99.7
80	85	3	37.10	17.57	-61.8		100.0
85	90	1					

[a]Arbitrary but consistent units.

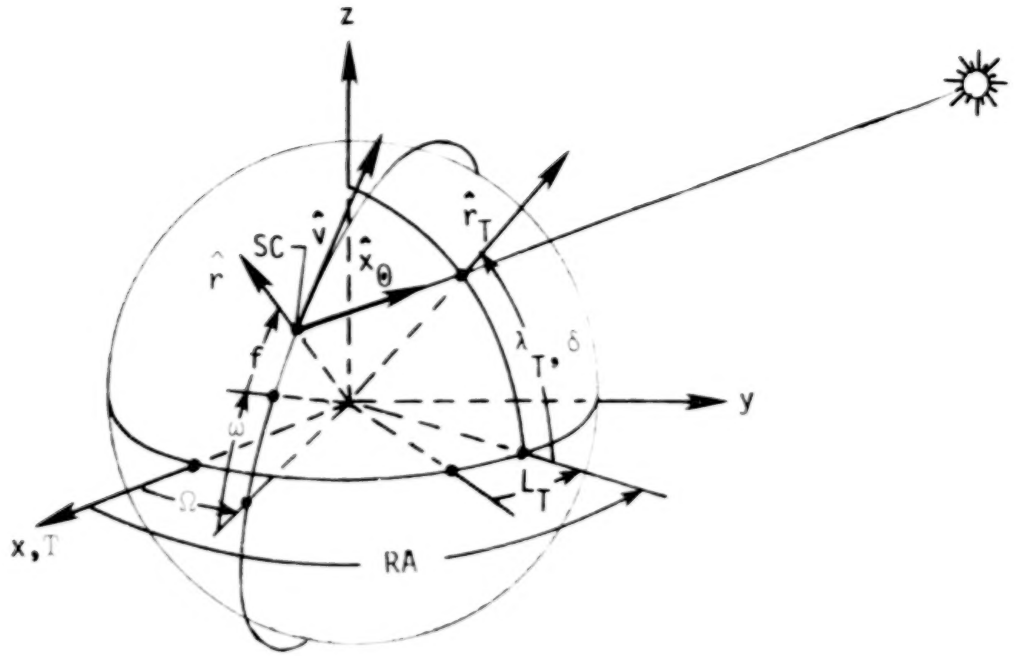

Figure 1.- Orbit geometry for viewing sunrises and sunsets from a spacecraft.

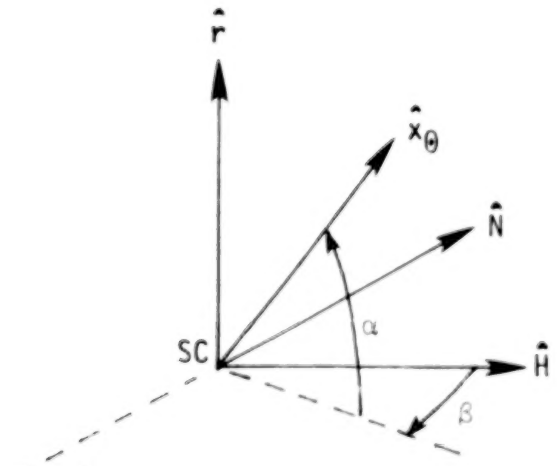

$\hat{N}$ = (sin Ω sin i, -cos Ω sin i, cos i)

$\hat{H}$ = ($\hat{N}$ x $\hat{r}$)

Figure 2.- Definition of pointing angles to the Sun relative to a spacecraft.

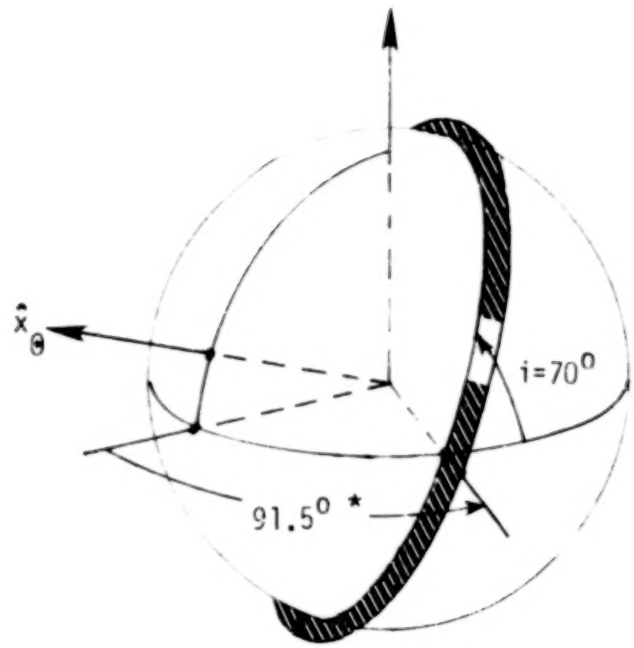

*Initial RA of orbit = 180°

RA of Sun at launch date = 88.5°

Figure 3.- Initial orbit geometry which results in a period of continuous sunlight viewed from a spacecraft.

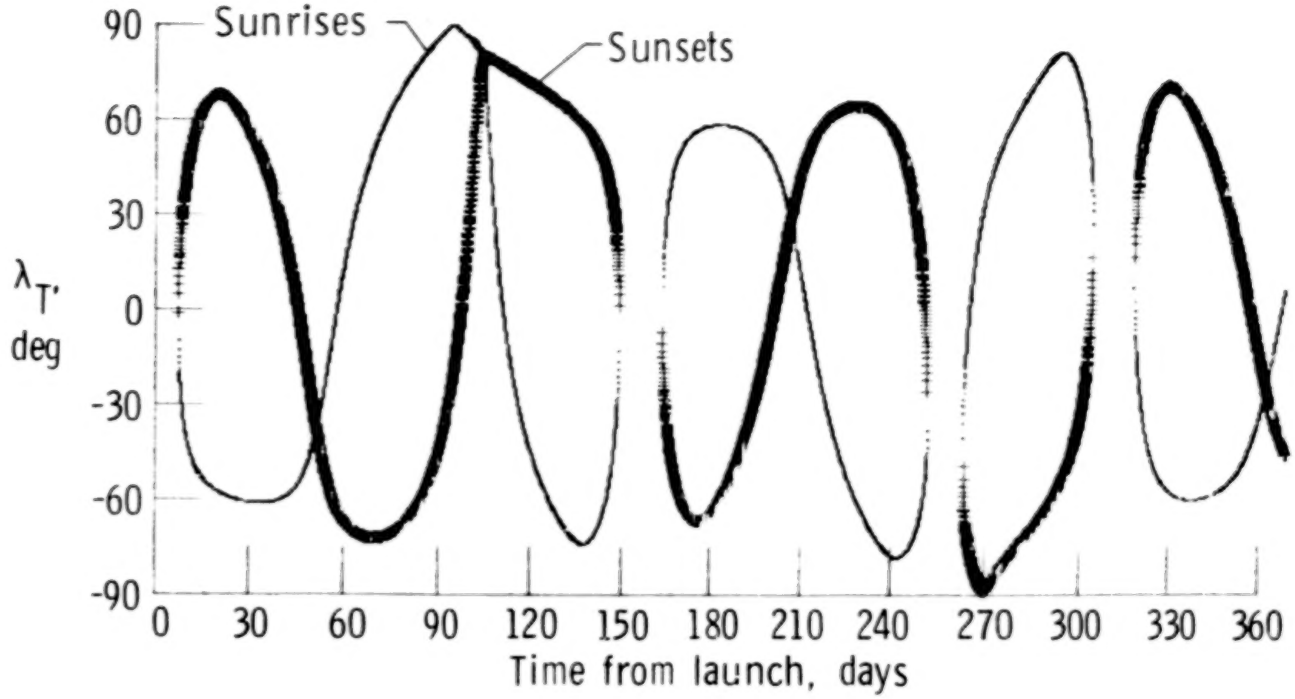

(a) Earth tangent latitude versus time from launch (see fig. 1).

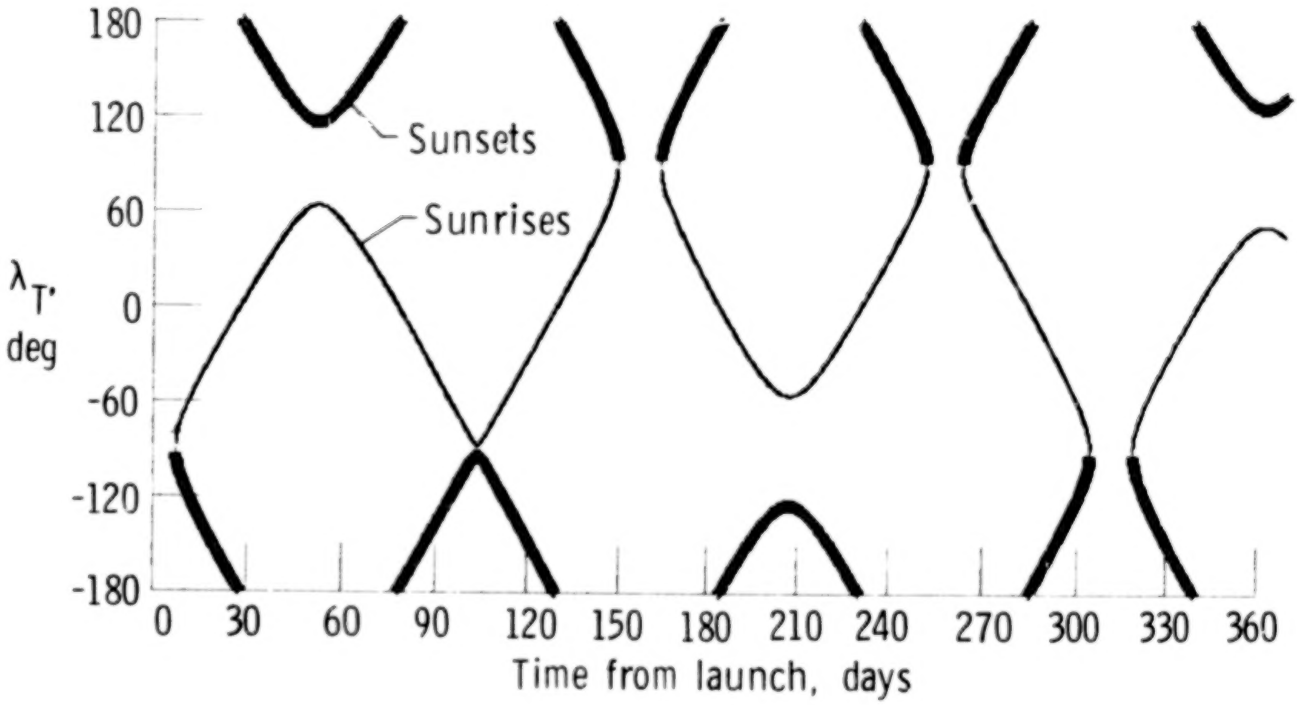

(b) Pointing angle β versus time from launch (see fig. 2).

Figure 4.- Orbital data for a 1-year solar occultation mission using a 70°, 600-km circular orbit.

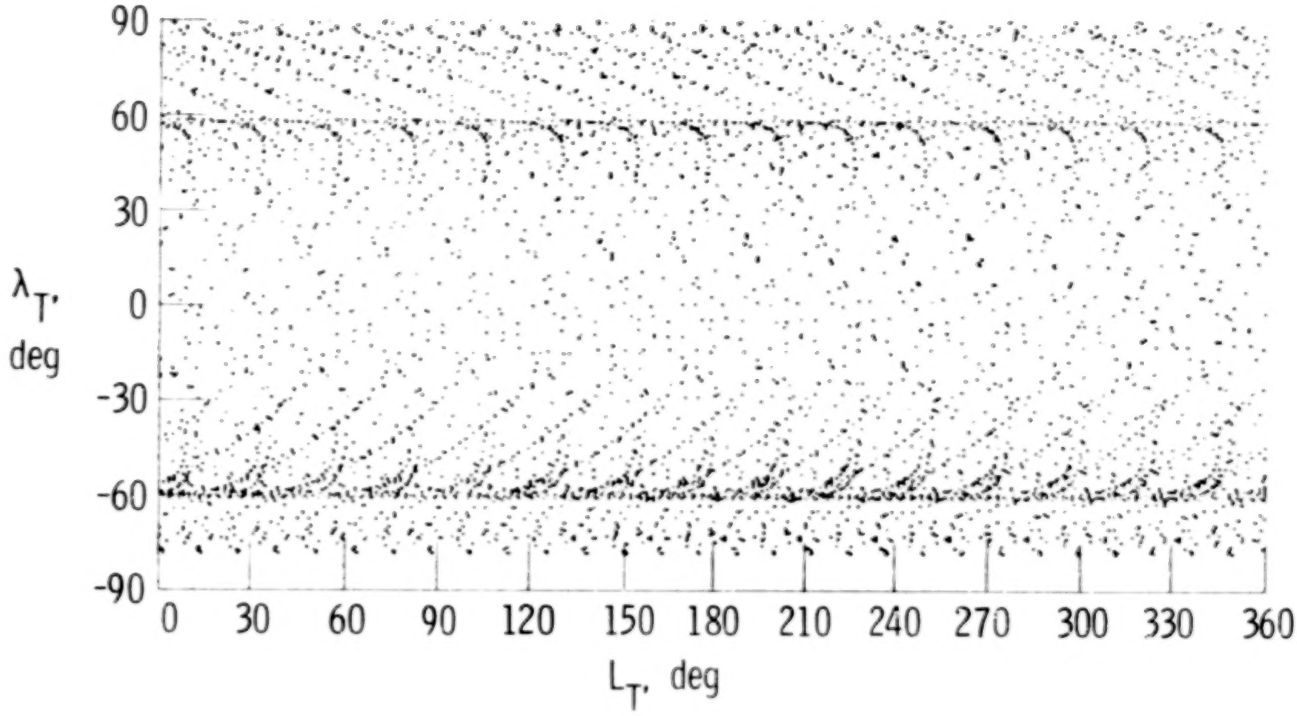

(c) Earth tangent latitude versus longitude for sunrises.

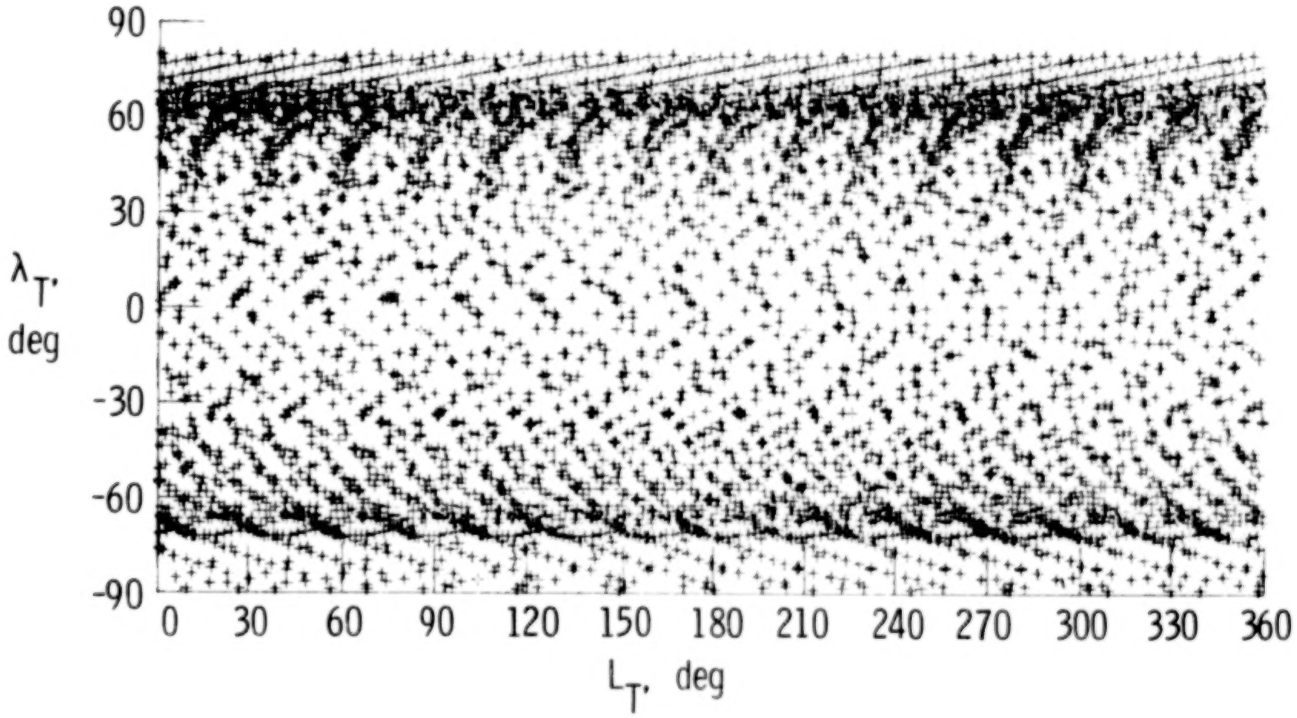

(d) Earth tangent latitude versus longitude for sunsets.

Figure 4.- Continued.

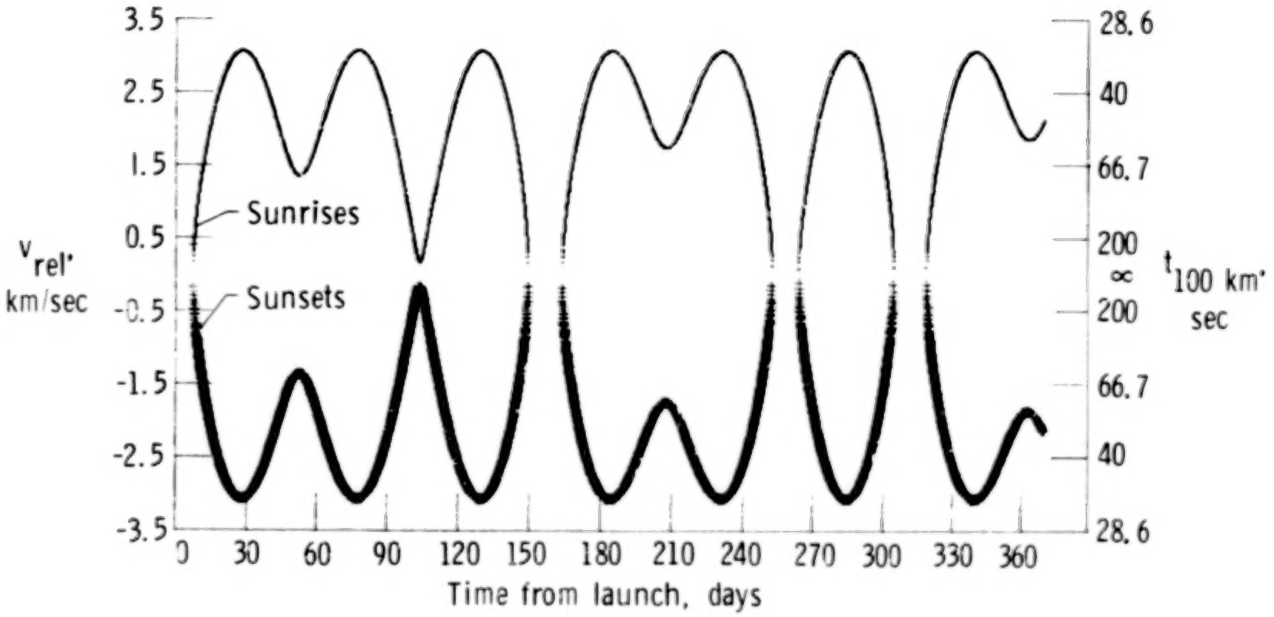

(e) Apparent vertical velocity of the Sun's image relative to the horizon at the instant of sunrise or sunset. t_{100} = Time to pass through 100 km at constant rate v_{rel}.

Figure 4.- Concluded.

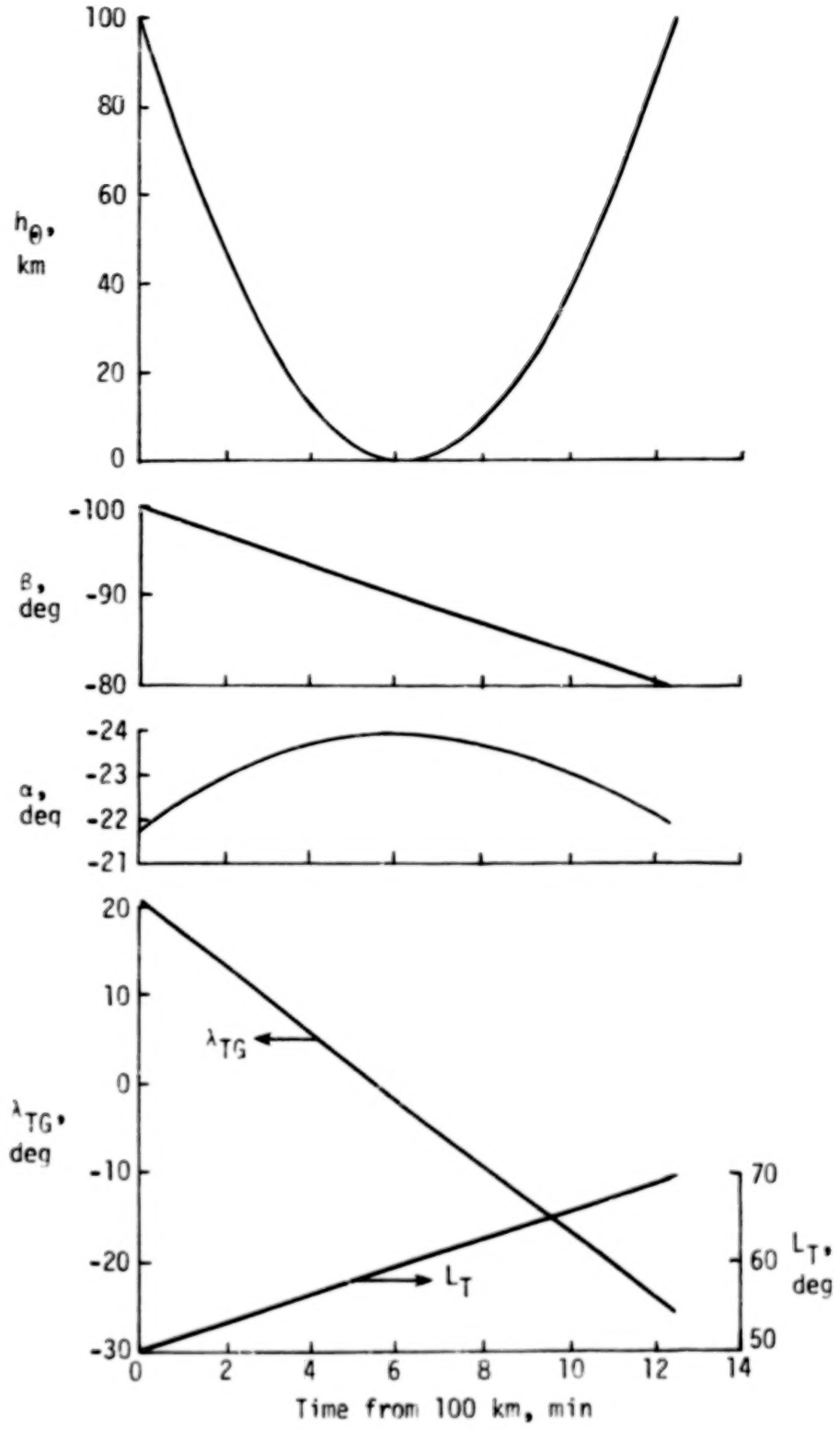

Figure 5.- Sun viewing requirements and surface coordinates during a solar sunset and sunrise near the beginning of a period of occultation (day 7 of the nominal mission). h_Θ = Altitude of center of Sun's image above the local horizon.

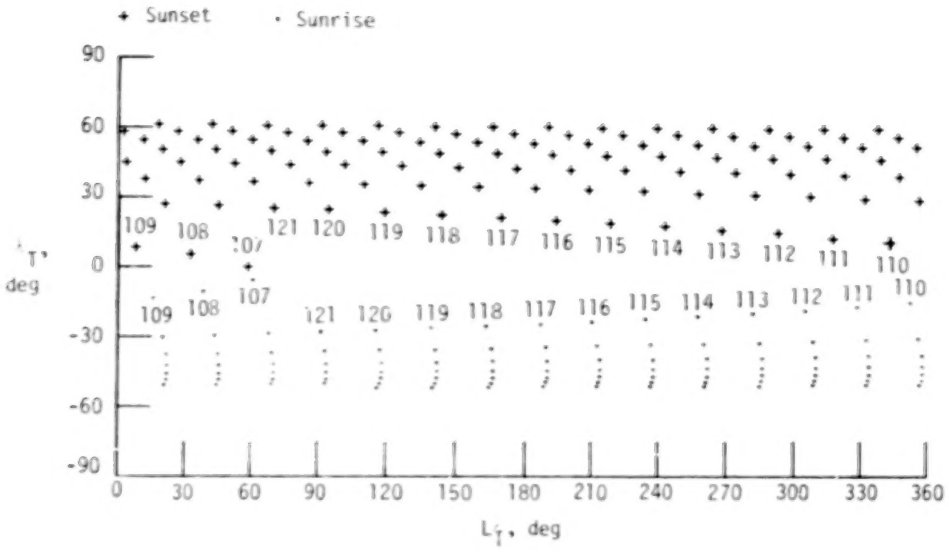

(a) During first 7 days after start of occultations.

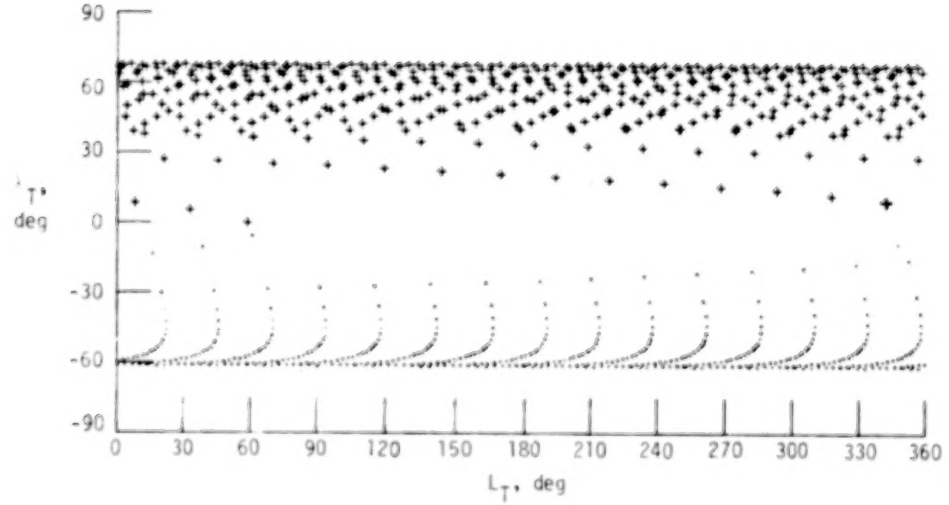

(b) During first 30 days after start of occultations.

Figure 6.- Tangent latitudes and longitudes of sunrises and sunsets during nominal mission.

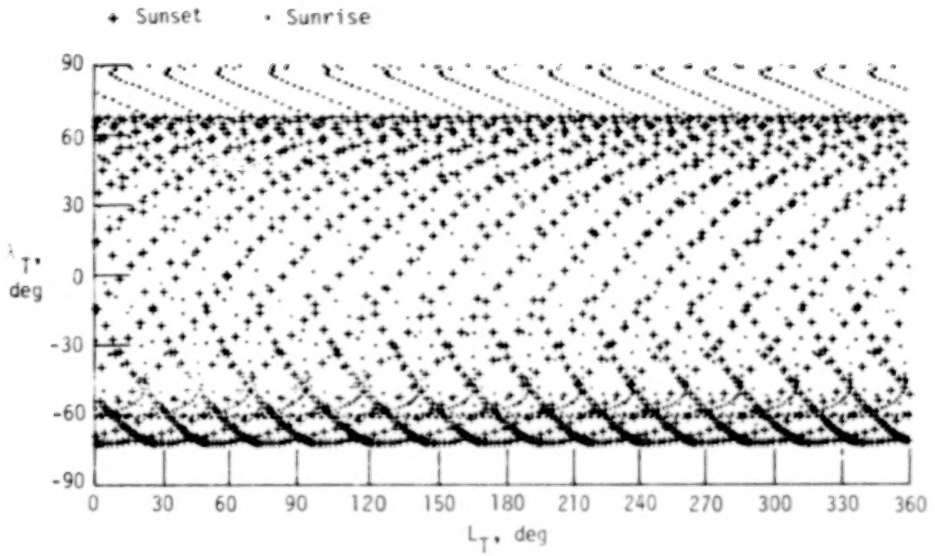

(c) During first 90 days after start of occultations.

Figure 6.- Concluded.

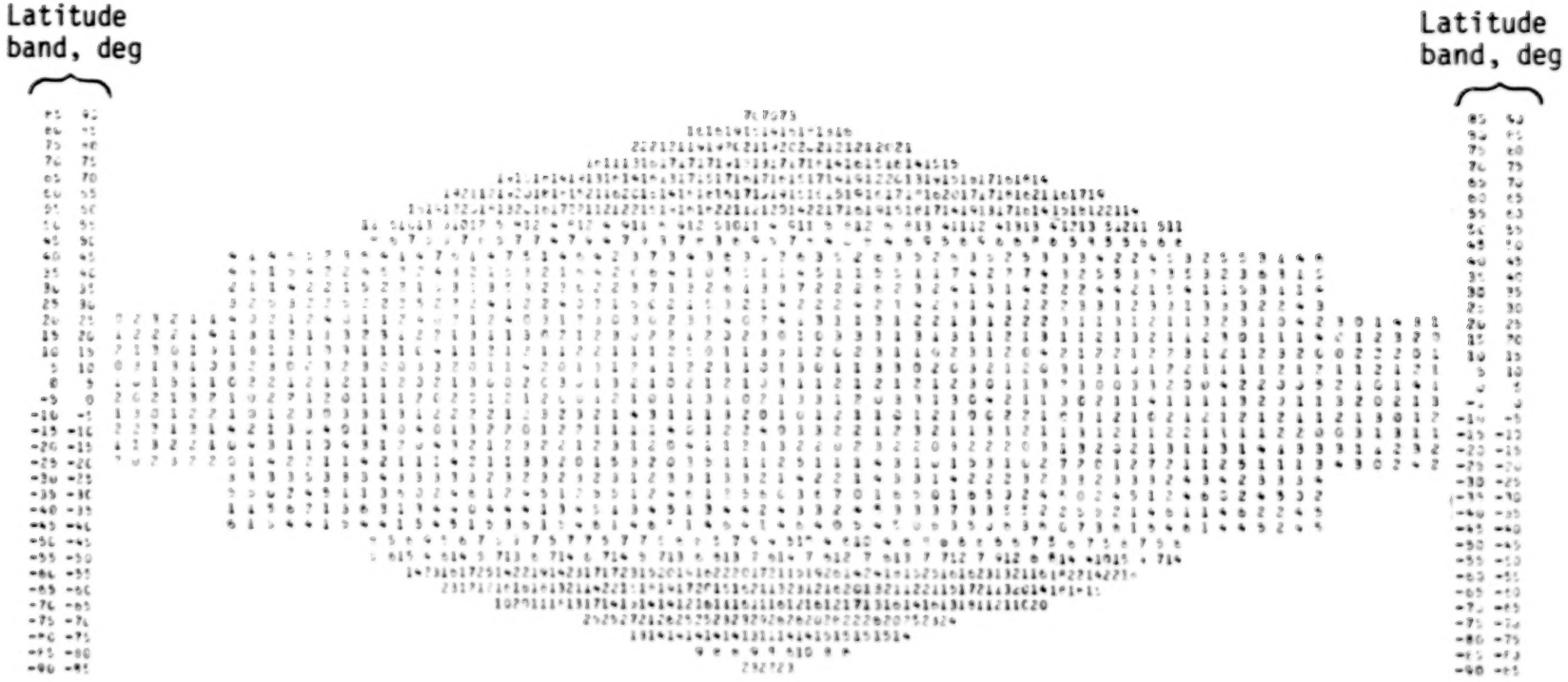

Figure 7.- Distribution of occultation measurements as a function of latitude and longitude boxes of approximately equal area (3×10^5 km^2) for the nominal solar occultation mission.

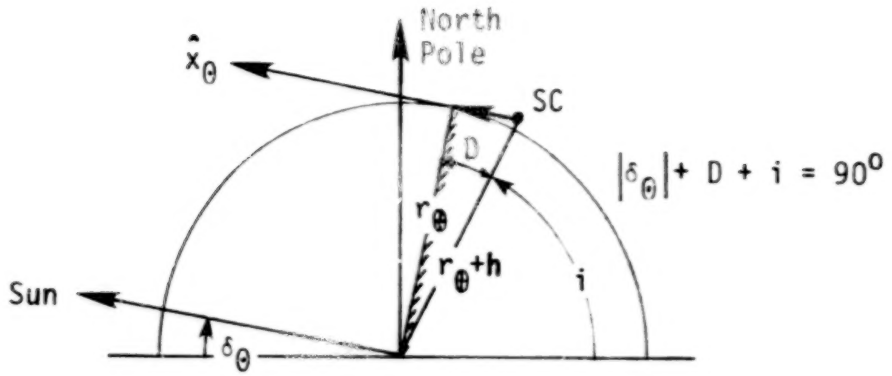

(a) Viewing periods of continuous sunlight given a value of solar declination.

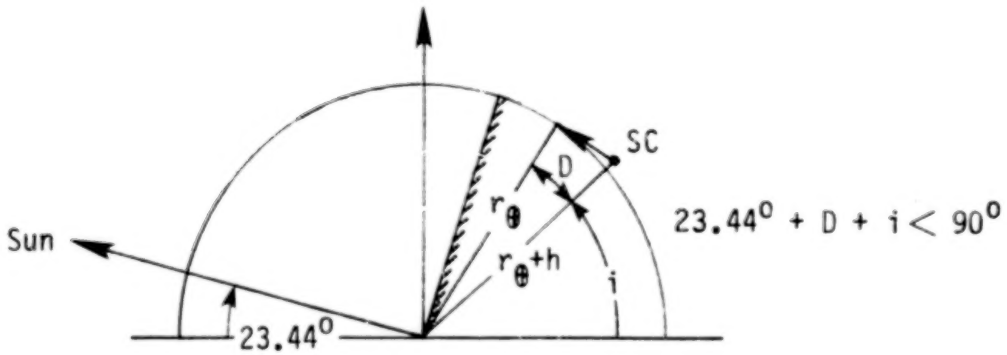

(b) Continuous sunlight never occurs.

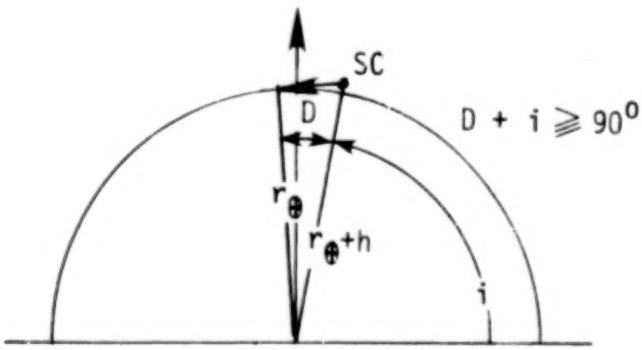

(c) Continuous sunlight is possible regardless of solar declination.

Figure 8.- Examples of limiting cases and geometries for viewing sunrises and sunsets from spacecraft orbits.

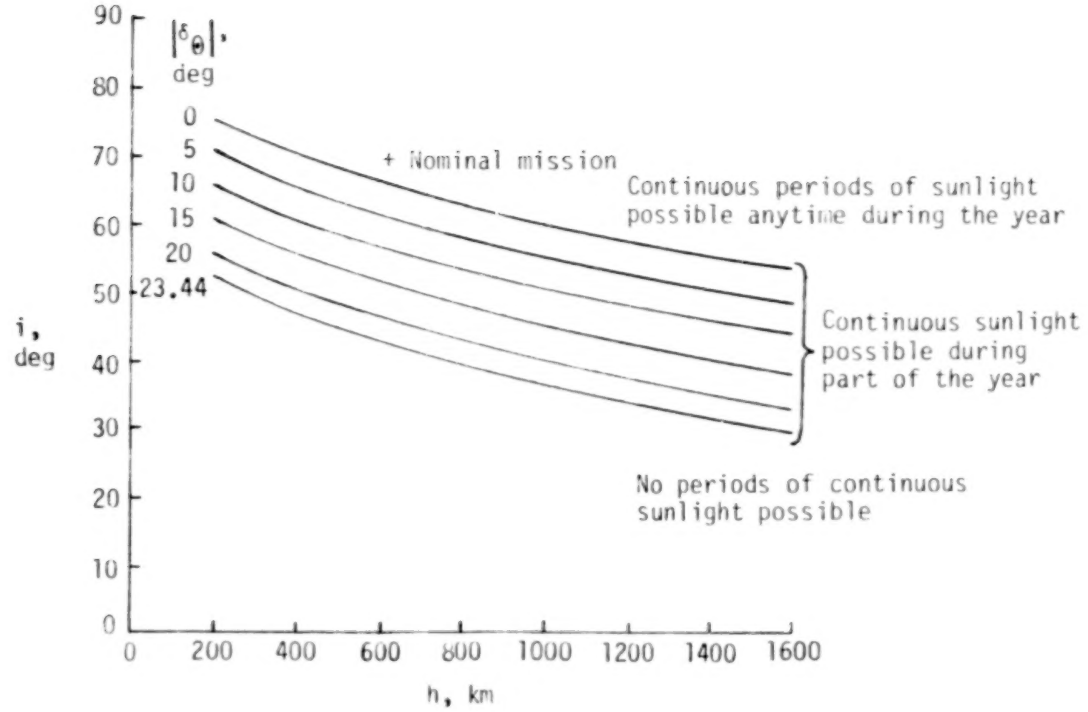

Figure 9.- Orbit and solar declination conditions required to produce periods of continuous sunlight during solar occultation missions.

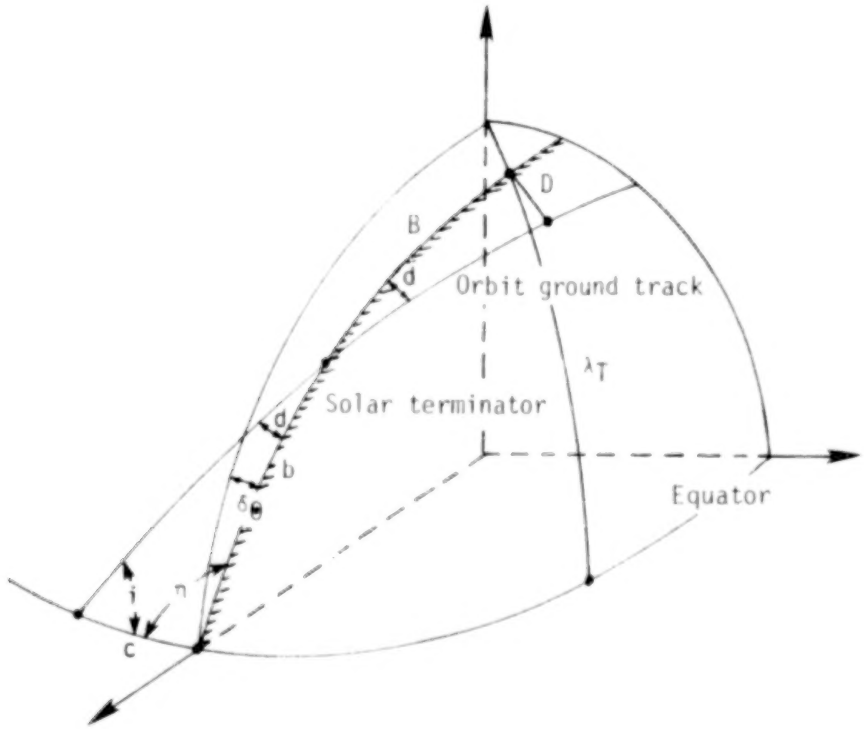

Figure 10.- Geometry for establishing the tangent latitude of a solar occultation measurement.

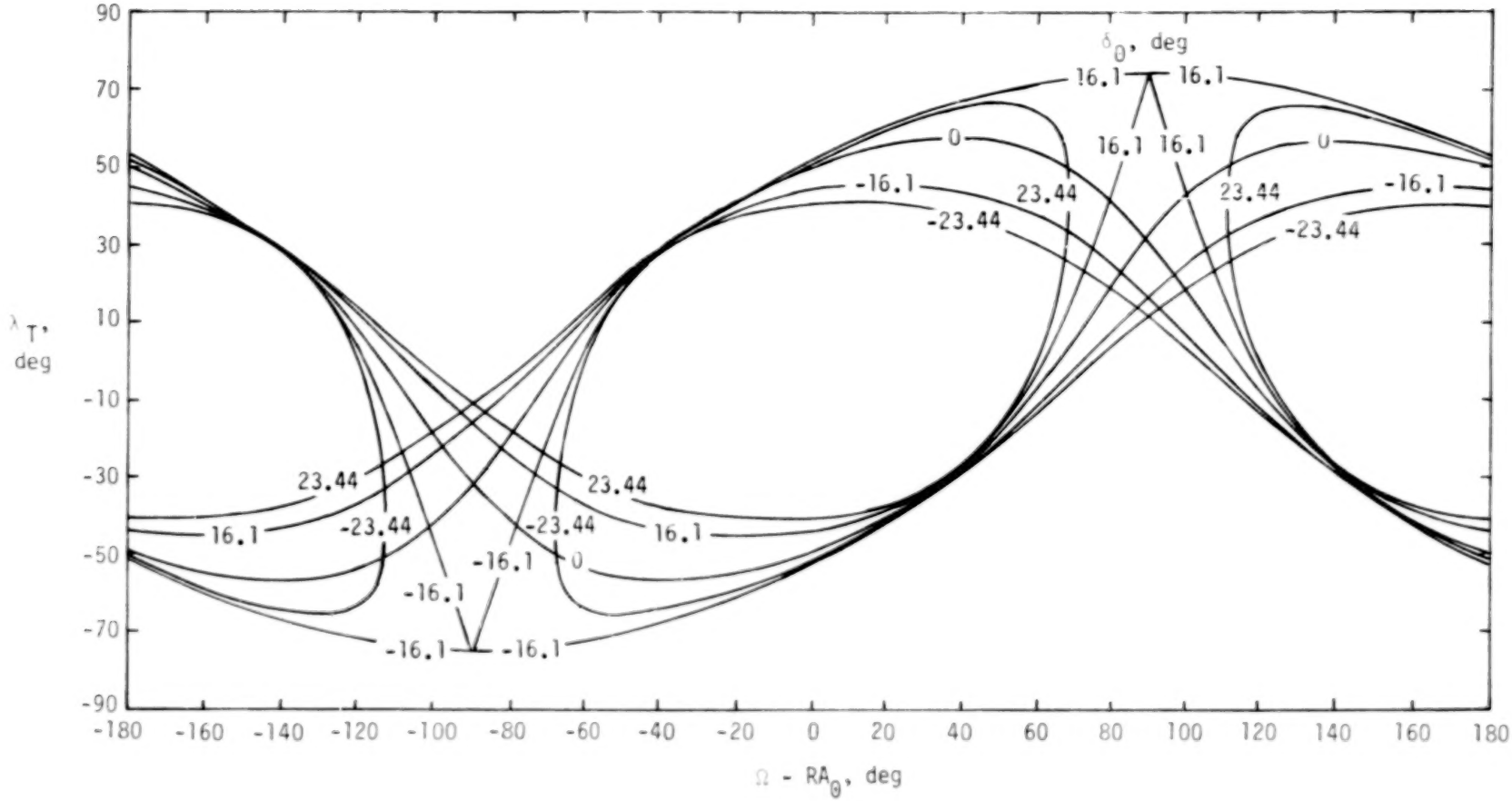

(a) $i = 50^\circ$.

Figure 11.- Tangent latitudes available during solar occultation missions for 50° and 70°, 600-km orbits as a function of orbit plane orientation relative to the Sun, with solar declination as a parameter.

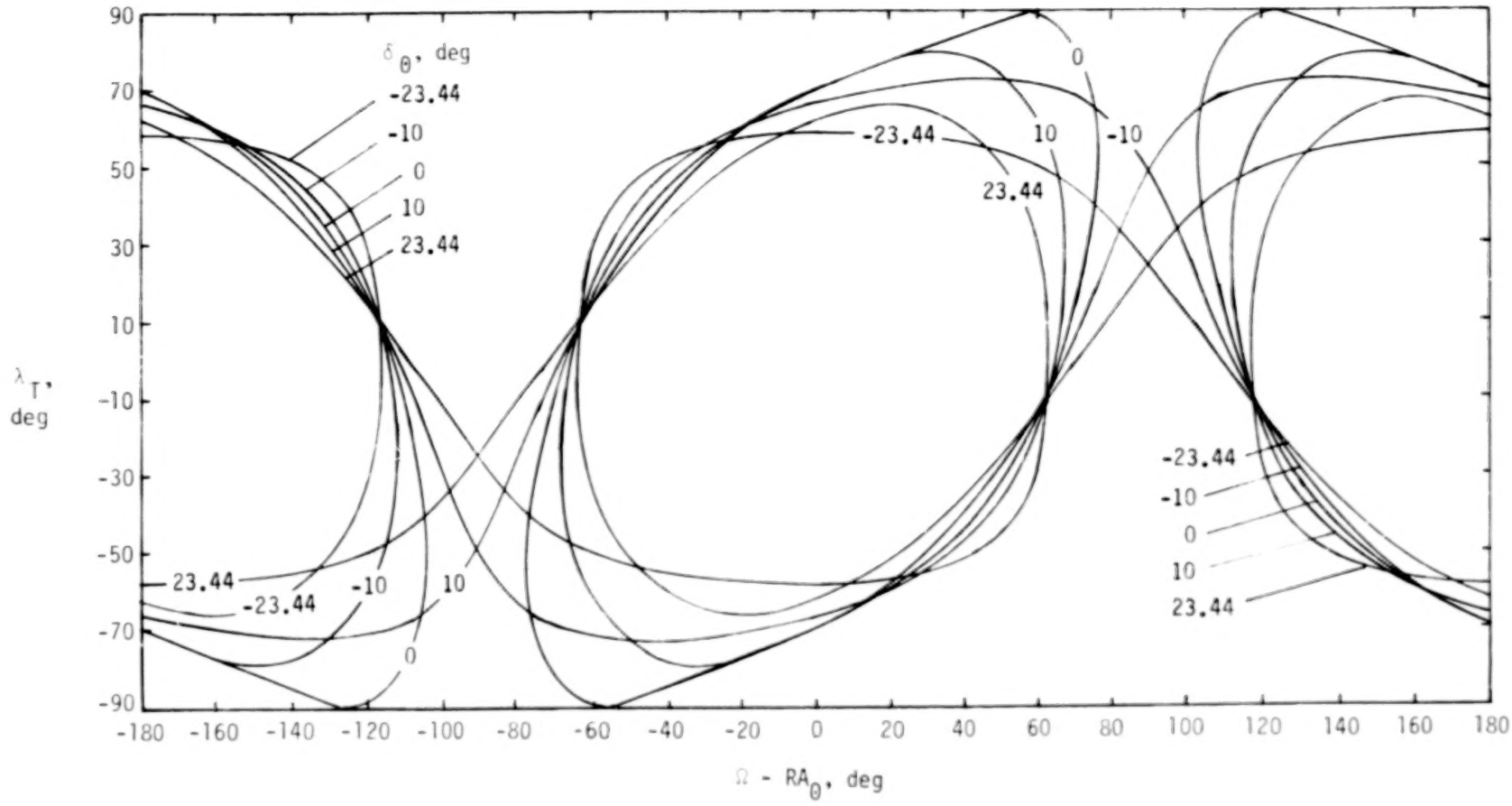

(b) $i = 70^\circ$.

Figure 11.- Concluded.

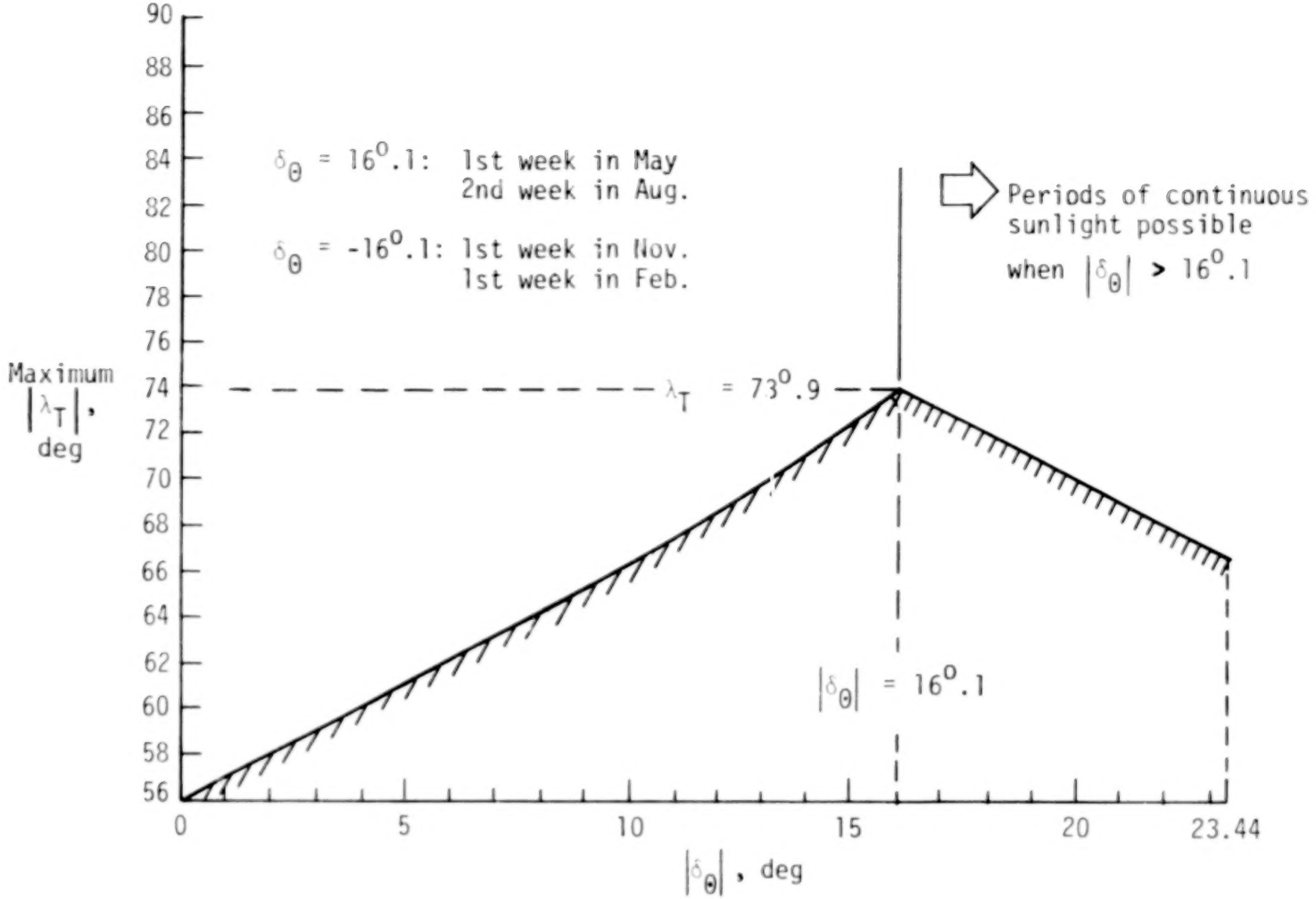

Figure 12.- Maximum latitude coverage available from a 50°, 600-km circular orbit as a function of solar declination.

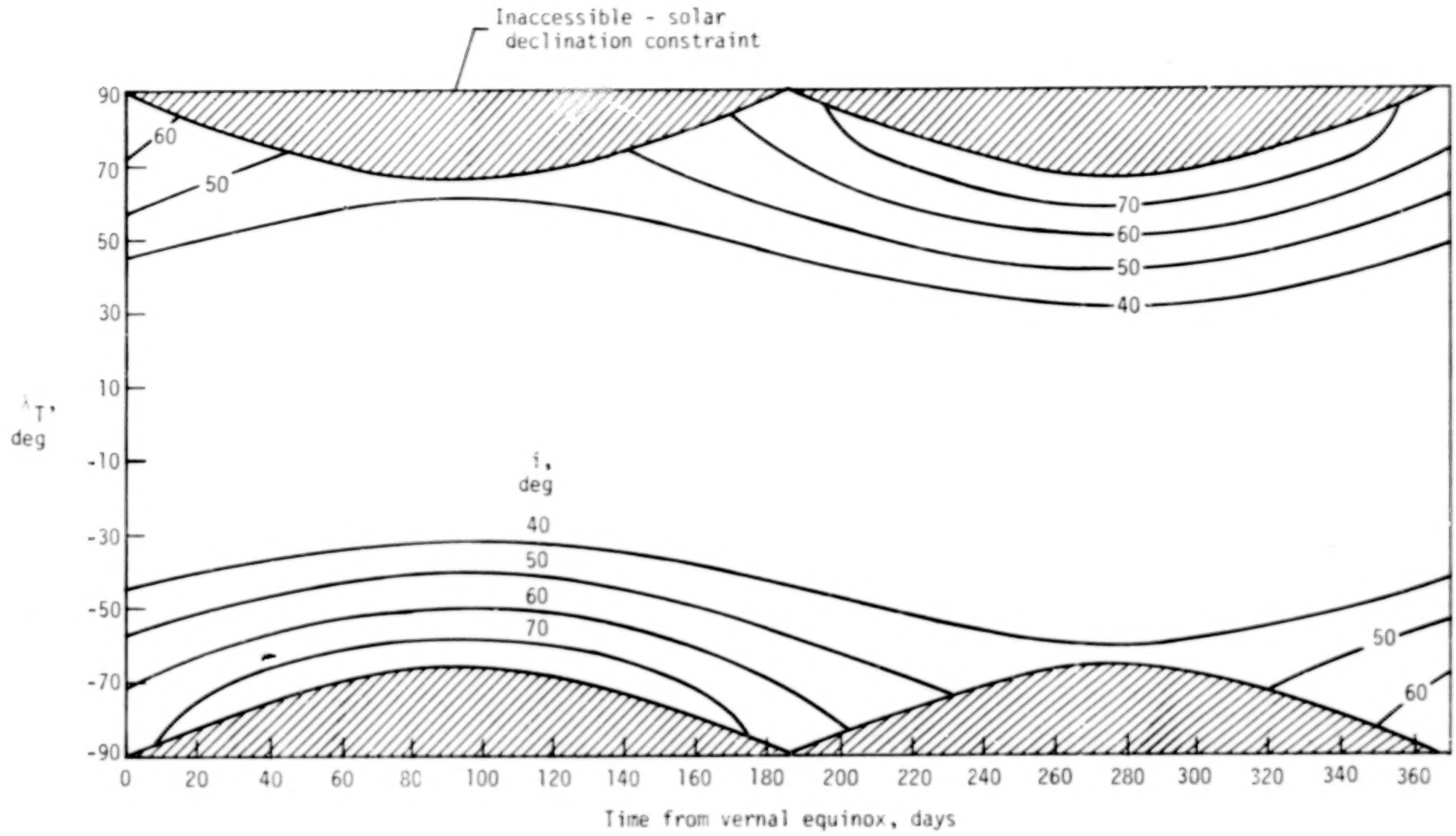

Figure 13.- Envelopes of tangent latitudes available during solar occultation missions at 600 km and various inclinations.

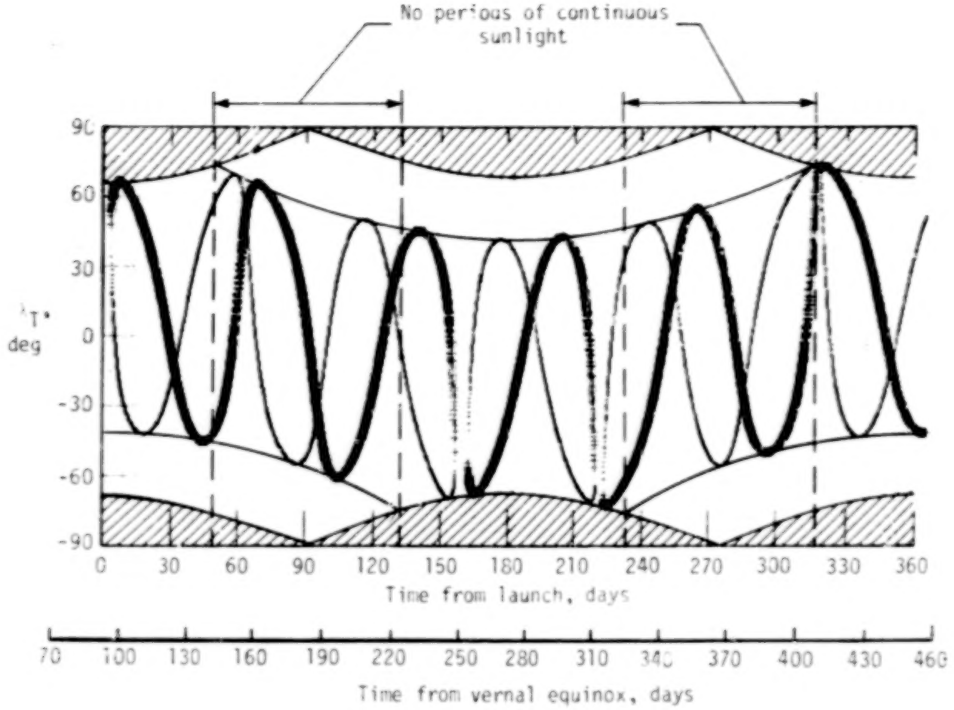

(a) Nominal orbit plane orientation to produce continuous sunlight at time of launch.

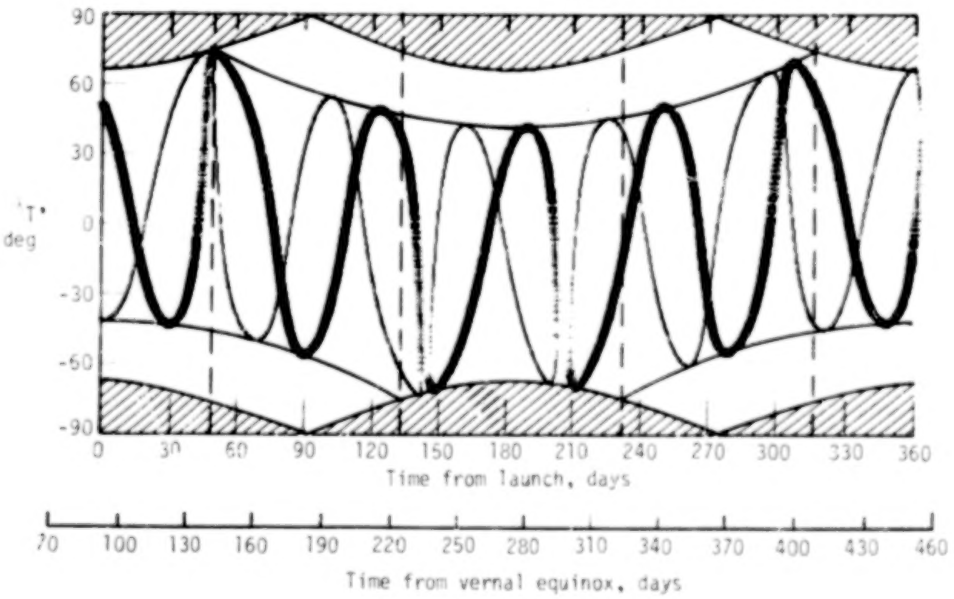

(b) Orbit plane rotated to produce sunrises and sunsets at time of launch.

Figure 14.- Solar occultation tangent latitude envelopes for 50°, 600-km orbits superimposed on two simulated 1-year missions.

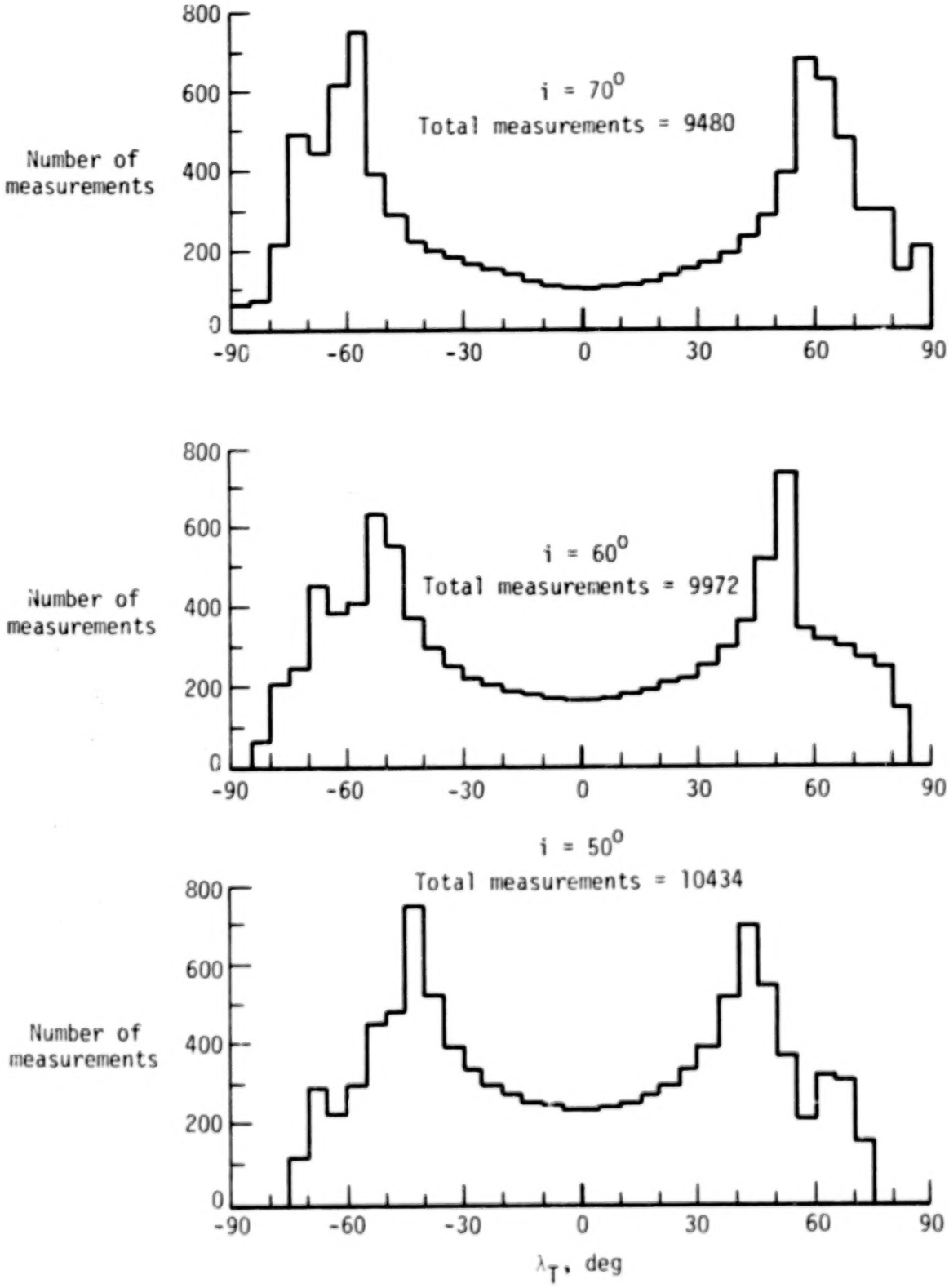

Figure 15.- Distribution of measurement (tangent) latitudes for 1-year simulated solar occultation missions in 600-km circular orbits.

1. Report No.	2. Government Accession No.	3. Recipient's Catalog No.
NASA TP-1606		

4. Title and Subtitle	5. Report Date
ORBIT DYNAMICS AND GEOGRAPHICAL COVERAGE CAPABILITIES OF SATELLITE-BASED SOLAR OCCULTATION EXPERIMENTS FOR GLOBAL MONITORING OF STRATOSPHERIC CONSTITUENTS	March 1980
	6. Performing Organization Code

7. Author(s)	8. Performing Organization Report No.
David R. Brooks	L-12804
	10. Work Unit No. 146-60-02-01

9. Performing Organization Name and Address	11. Contract or Grant No.
NASA Langley Research Center Hampton, VA 23665	

12. Sponsoring Agency Name and Address	13. Type of Report and Period Covered
National Aeronautics and Space Administration Washington, DC 20546	Technical Paper
	14. Sponsoring Agency Code

15. Supplementary Notes

16. Abstract

Orbit dynamics of the solar occultation technique for satellite measurements of the Earth's atmosphere are described. A 1-year mission is simulated and the orbit and mission design implications are discussed in detail. Geographical coverage capabilities are examined parametrically for a range of orbit conditions. The hypothetical mission is used to produce a simulated 1-year data base of solar occultation measurements; each occultation event is assumed to produce a single number, or "measurement," and some statistical properties of the data set are examined. A simple model is fitted to the data to demonstrate a procedure for examining global distributions of atmospheric constituents with the solar occultation technique.

17. Key Words (Suggested by Author(s))	18. Distribution Statement
Orbit dynamics Remote sensing Satellite monitoring Solar occultation	Unclassified - Unlimited Subject Category 13

19. Security Classif. (of this report)	20. Security Classif. (of this page)	21. No. of Pages	22. Price*
Unclassified	Unclassified	74	$5.25

* For sale by the National Technical Information Service, Springfield, Virginia 22161

NASA-Langley, 1980